1 Photochemical aging of guaiacol by Fe(III)-oxalate complexes in

2 atmospheric aqueous phase

23

3 Hongwei Pang¹, Qi Zhang², Hongli Wang³, Dongmei Cai¹, Yingge Ma³, Li Li³, 4 Kangning Li¹, Xiaohui Lu^{1*}, Hong Chen¹, Xin Yang^{1,4*}, Jianmin Chen¹ 5 6 ¹Shanghai Key Laboratory of Atmospheric Particle Pollution and Prevention, 7 Department of Environmental Science and Engineering, Fudan University, Shanghai 8 200433, China 9 ²Department of Environmental Toxicology, University of California, Davis, California 10 95616, United States 11 ³State Environmental Protection Key Laboratory of Formation and Prevention of the 12 Urban Air Pollution Complex, Shanghai Academy of Environmental Sciences, 13 Shanghai 200233, China 14 ⁴Shanghai Institute of Pollution Control and Ecological Security, Shanghai 200092, 15 16 China 17 Xiaohui Correspondence to: Lu (<u>luxiaohui@fudan.edu.cn</u>); Xin Yang 18 (yangxin@fudan.edu.cn) 19 20 21 22

Abstract:

24

25

26

27

28

29

30

31

32

33

34

35

36

37

38

39

40

41

Fe(III)-oxalate complexes are likely abundant in clouds, fogs and aerosol water. They are photoreactive and can act as an important source of reactive oxygen species (•OH, H₂O₂ and HO₂•) in tropospheric aqueous phases. Although the mechanisms involved in ferrioxalate photolysis have been investigated extensively, few kinetic and mechanistic information is available on the aging of dissolved organic compounds by this photochemical system. In this work, the Fe(III)-oxalate mediated photooxidation of guaiacol (GUA), a model for phenolic compounds emitted from biomass burning, was investigated under typical pH conditions of the atmospheric water. The effect of Fe(III) concentration, oxalate concentration and pH on the photooxidation of GUA was studied in detail. Our results revealed that oxalate can inhibit the oxidation of GUA by Fe(III) under the dark condition. However, the iron-catalyzed photooxidation of GUA can be strongly promoted in the presence of oxalate due to the formation of photoactive Fe(III)-oxalate complexes. GUA was rapidly oxidized to form a number of polymeric, functionalized and open-ring products with low volatility. Detailed reaction pathways for the photooxidation of GUA by Fe(III)-oxalate complexes were proposed based on the results of high-resolution mass spectrometry. This work suggests that ferrioxalate photochemistry can play an important role in the transformation of dissolved organics in atmospheric aqueous phases.

42 43

44

45 46 **Keyword:** Photooxidation, Iron oxalate, Guaiacol, Hydroxyl radical, Secondary organic aerosol, Atmospheric aqueous chemistry

1. Introduction:

Transition metals play an important role in the aging and transformation of inorganic and organic contents in atmospheric liquid phase.^{1, 2} Iron, the most abundant transition metal in the Earth's crust, has been identified as an important component in cloud and fog droplets.^{1, 3} The concentration of iron can range from micromolar to millimolar in cloud droplets and micromolar to tens of micromolar in fog waters, which is much higher than the concentrations of other transition metals.¹ Due to its significant concentrations and reactivity, iron can play a crucial role in chemical transformations of dissolved organics in atmospheric aqueous phases.^{4, 5} Several studies have reported the degradation of soluble organics via the photolysis of iron hydroxy complexes or through the Fenton reactions in atmospheric waters.^{4, 6, 7} The iron hydroxy complexes can undergo efficient photo-dissociation to form Fe(II) and 'OH under atmospherically relevant pH conditions (reaction 1 and 2), since they absorb in the near-UV region (290-400nm).⁸ The redox reaction of Fe(II) with H₂O₂ (Fenton reaction) can produce aqueous 'OH in the dark (reaction 3).

$$Fe(III) + H_2O \rightarrow [Fe(III)(OH)]^{2+} + H^+$$
 (1)

$$[Fe(III)(OH)]^{2+} + hv \rightarrow Fe(II) + OH \qquad k = 0.0012 \text{ s}^{-1} \qquad \text{ref.}^{9}$$
 (2)

$$Fe(II) + H_2O_2 \rightarrow Fe(III) + \cdot OH + OH^- \quad k = 76 \text{ M}^{-1} \text{ s}^{-1} \quad \text{ref.}^{10}$$
 (3)

In addition to hydroxy complexes, iron can form organic complexes that are photochemically reactive and can initiate radical chain reactions. For example, a recent study has shown that the iron-carboxylato complexes formed between iron and low-molecular-weight carboxylates can have a profound impact on the iron-catalyzed photooxidation of soluble organic pollutants in atmospheric waters. 11 Carboxylates are often found in significant concentrations in atmospheric waters and tend to dominate the complexation of Fe(III) ions due to the large stability constants of such complexes. 12 Oxalate, one of the most abundant low-molecular-weight carboxylates in atmospheric waters, forms chelate complexes with Fe(III) efficiently. Zuo et al. found that Fe(III)-oxalate complexes can be the dominant species of dissolved Fe(III) in many atmospheric water samples because oxalate has a stronger affinity for Fe(III) than most of other organic ligands typically present in atmospheric droplets. 13, 14 Fe(III)-oxalate complexes are typically more photoactive than "unchelated" Fe(III) ions because complexation yields a stronger absorbing chromophore, which is derived from electron transfer from oxalate ligand to iron(III).¹⁵ The photo-reactions of Fe(III)-oxalate complexes have significant implications for iron redox cycle and are

potentially an important source of oxidative species in the atmosphere.

90

91

92

93

94

95

96

97

98

99

100

101

102

103

104

105

106

107

108

109

110

111

112

113

114

115

The proposed mechanisms for the photochemical/chemical generation of oxidative species from Fe(III)-oxalate complexes are shown in reactions 4-9 below.

84
$$[Fe(III)(C_2O_4)_3]^{3-} + hv \rightarrow [Fe(II)(C_2O_4)_2]^{2-} + C_2O_4^{--}$$
 $k = 0.04 \text{ s}^{-1}$ ref. 9 (4)
85 $C_2O_4^{--} \rightarrow CO_2^{--} + CO_2$ $k = 2 \times 10^6 \text{ s}^{-1}$ ref. 16 (5)
86 $CO_2^{--} + O_2 \rightarrow CO_2 + O_2^{--}$ $k = 6.5 \times 10^9 \text{ M}^{-1} \text{ s}^{-1}$ ref. 17 (6)
87 $O_2^{--} + H^+ \leftrightarrow HO_2^{--}$ (7)
88 $Fe(II) + O_2^{--}/HO_2^{--} + H^+ \rightarrow Fe(III) + H_2O_2$ $k = 1.0 \times 10^7/1.2 \times 10^6 \text{ M}^{-1} \text{ s}^{-1}$ ref. 18 (8)
89 $[Fe(II)C_2O_4] + H_2O_2 \rightarrow [Fe(III)C_2O_4]^+ + \cdot OH + OH^ k = 3.1 \times 10^4 \text{ M}^{-1} \text{ s}^{-1}$ ref. 19 (9)

Depending on the pH and the Fe(III)/oxalate ratio, oxalate forms three kinds of complex with Fe(III): $[Fe(III)(C_2O_4)]^+$, $[Fe(III)(C_2O_4)_2]^-$ and $[Fe(III)(C_2O_4)_3]^{3-}$, simultaneously in different proportions in solution. 20 [Fe(III)(C₂O₄)₂] and [Fe(III)(C₂O₄)₃]³⁻ are known to have a higher photochemical reactivity than [Fe(III)(C₂O₄)]⁺. ²¹ Among Fe(III)-oxalate complexes, the photodissociation of $[Fe(C_2O_4)_3]^{3-}$ is of most intense interest and has been investigated in detail. The primary photochemical process following the excitation of $[Fe(C_2O_4)_3]^{3-}$ involves intramolecular electron transfer from oxalate to Fe(III) with formation of a primary intermediate C₂O₄ (reaction 4), the C₂O₄ radical will then dissociate to form carbon dioxide anion radical (CO₂*-) and CO₂ instantly (reaction 5).²²⁻²⁴ The mechanism of photolysis of $[Fe(III)(C_2O_4)_2]^-$ and $[Fe(III)(C_2O_4)]^+$ has not been studied extensively but the reactions are assumed to produce Fe(II) and CO₂*- eventually.¹⁷ The subsequent reaction of CO2 with O2 leads to the formation of the intermediate superoxide ion and the hydroperoxyl radical (denoted as $O_2^{\bullet-}/HO_2^{\bullet}$), which reacts with Fe(II) to produce H₂O₂ in the acidic pH range (reaction 6-8). Finally, H₂O₂ will interact with Fe(II) (reaction 3) or with [Fe(II)C₂O₄] (reaction 9) to yield •OH.

Although the photochemistry of ferrioxalate complexes has been studied extensively, their role in the aging of atmospherically relevant species in aqueous phase is still in its infancy.¹¹ Thomas et al. investigated the reactive uptake and photooxidation of gas-phase glycolaldehyde on aqueous seed aerosol containing Fe(III)-oxalate complexes.¹¹ They found that the presence of Fe(III)-oxalate in seed aerosol inhibited the aerosol growth, which suggests that iron(III) oxalate-mediated photooxidation of glycolaldehyde leads to the formation of volatile oxidation products. Zuo et al. studied the Fe(III)-catalyzed photochemical oxidation of dissolved sulfur dioxide (SO₂) in the presence of oxalate under atmospherically relevant conditions.²⁵ Their results show that the presence of oxalate strongly inhibits Fe(III)-catalyzed

oxidation of SO₂ both in the dark and under UV-visible light due to the formation of Fe(III)-oxalate complexes. These works alluded to the potential importance of ferrioxalate photochemistry in atmospheric waters, but more studies are needed to better understand the role that Fe(III)-oxalate complexes may play in the evolution of dissolved organics.

This study explores the photochemical oxidation of guaiacol (GUA) in the presence of Fe(III)-oxalate under acidic conditions typical for atmospheric water. Guaiacol is chosen as a model compound of phenols, which are emitted in large quantities from biomass burning.²⁶ This work is the first to present comprehensive mechanistic and kinetic information on the photooxidation of guaiacol by Fe(III)-oxalate complexes under conditions relevant to atmospheric water. The effects of pH, Fe(III) concentration, oxalate concentration, and dissolved oxygen on the photooxidation of guaiacol were investigated. The photodegradation mechanism and the possible oxidative products were studied by high-resolution mass spectrometry (HRMS) combined with high performance liquid chromatography (HPLC). The results obtained in this study will provide a reference for predicting the photooxidation behavior of phenolic compounds in the presence of Fe(III)-carboxylato complexes in atmospheric water.

134135

136

137

138

139

140

141

142

143

144

145

146

147

148

116

117

118

119

120

121

122

123

124

125

126

127

128

129

130

131

132

133

2. Experimental section:

All photochemical experiments were conducted in a 200ml, airtight square quartz vessel (8 cm in length, containing 100ml solution) equipped with magnetic agitation and a bubble tube for feeding high-purity air or nitrogen. For the deaeration experiment, the solution was continuously bubbled with high-purity N_2 starting from 15 min before the reaction till the end of the photoreaction. A 500W Xe lamp was used as irradiation source to simulate sunlight outside the reactor at 4 cm distance from the reactor walls. The Xe lamp with a polychromatic spectrum of $\lambda \geq 350$ nm was selected in order to avoid the direct photolysis of GUA. The irradiance at the surface of the solutions was measured at approximately 980 W m⁻², which is equivalent to sunlight intensity at mid-latitude summer noon, as estimated by ferrioxalate actinometry. The solution temperature of the reaction vessel was kept at 25±2 °C by means of a cooling fan during the experiment. NaCl (2.58×10⁻³ M) was added to keep the ionic strength constant throughout each experiment. The materials,

reagents and additional experimental details are provided in the Supporting Information.

The concentrations of GUA and nitrobenzene were determined by HPLC. 28 The experimental error in the HPLC analytical measurements is < 2% on the basis of triplicate runs. The oxidation products of GUA were analyzed and formula-assigned by an Orbitrap HRMS (mass resolution m/ Δ m =140000) equipped with HPLC. As a control experiment, 1 mM GUA (pH 3.0) was directly infused into HRMS to investigate if autoxidation of GUA occurs in the ESI source. According to the study of Slikboer et al.,⁵ catechol can be oxidized to formed hydroxylated quinone species (autoxidation product) under electrospray ionization conditions in the presence of O₂(aq). However, no autoxidation product of GUA was observed in our system. The reason may be that GUA is less susceptible to oxidation in the ESI source compared to catechol. The light absorptivity of the solution and the concentration of H₂O₂ were measured by UV-vis spectroscopy. In addition, gas chromatography/mass spectrometry (GC-MS) was applied to detect the low-molecular-weight products of reactions (e.g., methanol). All speciation calculations in this work were carried out with a chemical equilibrium calculation program - Visual MINTEQ (developed by KTH, SEED, Stockholm, Sweden). Details on the analytical procedures are given in the Supporting Information.

3. Results and discussion:

3.1. Effects of oxalate on the dark iron-oxidation of GUA in aqueous solutions

Recently, several studies have reported that the dark reaction of Fe(III) with GUA can result in the formation of light-absorbing insoluble and soluble secondary organics in aqueous solution at pH 3 under experimental conditions representative of atmospheric water.^{5, 29} Figure 1 and Figure S1a show the UV-vis absorption spectra of the solution resulting from the dark reaction of GUA with Fe(III) at pH = 3 in the presence of air. The development of a wide absorption band extending from the UV region (350 nm) to the visible region (600 nm) in the dark solution of GUA + Fe(III) is attributed to the formation of conjugated oligomer products of GUA (such as compound II in Figure S2).⁵ The proposed reaction mechanism involves the oxidation of GUA by Fe(III) to form the corresponding phenoxy radical, which proceeds through carbon-carbon radical coupling to form guaiacol dimer and the respective

diphenoquinone (Figure S2). Interestingly, the formation of insoluble secondary organics was not observed in the dark solution of GUA + Fe(III), maybe due to the lower concentrations of Fe(III) and GUA used in this study. However, when oxalate was mixed with the Fe(III) and GUA at pH = 3, the broad absorption peak between 350 nm and 600 nm didn't appear in the UV-vis spectrum of the solution after 2 hours in the dark (Figure 1), indicating no formation of the light absorbing oligomers. Instead, the UV-vis spectrum shows an absorption tail extending into wavelength > 400 nm, so is the spectrum of the Fe(III) + oxalate solution (Figure 1). This tail is attributed to the ligand-to-metal charge transfer of the Fe(III)-oxalate complexes formed in both solutions. These results revealed that the presence of oxalate inhibited the dark reaction of GUA with Fe(III), likely through reducing the concentration of available Fe(III) species due to the formation of stable Fe(III)-oxalate complexes in the dark.

Significant concentrations of oxalate have been found in rain, cloud and fog waters, ¹³ for which the possible sources include the dissolution of gas-phase oxalate due to its large Henry's coefficient and aqueous-phase oxidation of organic compounds. In acidic atmospheric water, oxalate ligands readily form strong chelate complexes with Fe(III) ions, thus inhibit the dark Fe(III)-oxidation of dissolved organics (such as phenols) in aqueous phase. Our results demonstrate that in the presence of carboxylic acid ligands the dark Fe(III)-oxidation pathway may be less important for the transformation of phenolic compounds in atmospheric water.

3.2. Fe(III)-oxalate mediated photooxidation of GUA in aqueous solutions

3.2.1. The control experiments

Figure 2 shows the change of GUA concentration in aqueous solutions during the course of illumination in the presence or absence of Fe(III), and oxalate. No direct photooxidation of GUA is observed under the simulated sunlight conditions of this study ($\lambda > 350$ nm) because GUA in water does not absorb above 350 nm. In the presence of Fe(III) ions, the photooxidation of GUA occurred in the aqueous solution at pH 3. This is because Fe(OH)²⁺ is the dominant Fe(III) hydroxide complexes in the aqueous solution in the pH range of 3-5 and its charge transfer band overlaps the solar UV spectrum (290-400 nm).⁸ Thus under the simulated sunlight conditions, Fe(OH)²⁺ can be photolyzed to generate •OH radicals (reaction 2), which react with GUA via

electrophilic addition to form hydroxylated-oxidation products. Moreover, the initial photooxidation of the GUA-Fe(III) solution can be described using pseudo-first order kinetics with a rate constant of 0.004 min⁻¹ (Figure S3). Previous studies have demonstrated that 3 is the optimum pH value for Fe(III) hydroxide complexes to produce OH and oxidize the organic compounds without the precipitation of Fe(III).^{30, 31} As shown in Figure 2, the photo-degradation rate of GUA was further enhanced by adding oxalate into the aqueous solution containing GUA and Fe(III). The initial pseudo-first-order rate constant of GUA decay increased to 0.026 min⁻¹. approximately 6.5 times the rate observed in the illuminated GUA-Fe(III) solution (Figure S3). At the end of the irradiation (100 min), nearly 80% of the GUA in the GUA-Fe(III)-oxalate solution reacted compared to 17% in the GUA-Fe(III) solution (Figure 2). These results indicate that oxalate significantly promotes Fe-catalyzed photooxidation of GUA. The reason is that oxalate outcompetes hydroxide for complexation with Fe(III) in the acidic solution, which leads to a higher abundance of Fe(III)-oxalate complexes than Fe(III)-OH complexes in the solution and thereby alters the photoreduction pathways of Fe(III) and concomitantly the pathways of •OH formation.²⁴ Indeed, previous studies have indicated that Fe(III)-oxalate complexes have a much stronger light absorbance in the tropospheric solar UV-visible region and are photochemically more reactive than inorganic Fe(III) species such as Fe(OH)²⁺ in aqueous solution.9, 21 The photolysis of Fe(III)-oxalate complexes can efficiently produce OH in the presence of dissolved oxygen via a series of reactions (reaction 3-9), and the production rate is much higher than that of the Fe(III)-OH complexes.³¹, ³² The steady-state concentrations of •OH generated by photolysis of Fe(III)-oxalate complexes and Fe(III)-OH complexes were measured employing nitrobenzene (NB) as a 'OH trap.33 The photodegradation of NB can be described using pseudo-first-order kinetics in terms of [NB] and the concentration of 'OH was estimated using the following equations:

216

217

218

219

220

221

222

223

224

225

226

227

228

229

230

231

232

233

234

235

236

237

238

239

240

241

242

248

$$\ln \frac{[NB]_0}{[NB]_t} = kt = k_{NB,OH} [OH] t$$
(10)

$$[\cdot OH] = \frac{k}{k_{NB,OH}} \tag{11}$$

Where [NB]₀ is initial NB concentration, [NB]_t is NB concentration at irradiation time t, and k and $k_{NB,OH}$ (= 3 × 10⁹ M⁻¹s⁻¹)³⁴ are the pseudo-first-order and second-order rate constants of NB reaction with •OH, respectively.

Figure S4 shows the photodegradation of NB in the presence of Fe(III)-oxalate

complexes and in the presence of Fe(III)-OH complexes. The degradation rate constant of NB in Fe(III)-oxalate system was found to be 0.045 min⁻¹, based on Eq. (11), [•OH] was calculated to be 2.5×10⁻¹³ M. Similarly, [•OH] was calculated to be 1.17×10⁻¹³ M in the irradiated Fe(III)-OH system. Hence, a higher efficiency of photooxidation of GUA was achieved in the aqueous solution containing Fe(III)-oxalate complexes compared to that containing the Fe(III)-OH complexes.

3.2.2. Effects of oxalate concentration on the Fe(III)-oxalate mediated photooxidation of GUA in aqueous solutions

The effect of oxalate concentration on the photooxidation of GUA was investigated from 20 to 250 μ M at a constant Fe(III) concentration of 20 μ M and pH = 3.0 under the simulated sunlight conditions. The photooxidation of GUA at different oxalate concentration is presented in Figure 3a as a function of irradiation time. The results indicate that an increasing concentration of oxalate, or molar ratio of oxalate to Fe(III), leads to a significant increase of the photooxidation efficiency of GUA. For example, the most effective degradation was observed at an oxalate concentration of 250 μ M with a loss of \approx 80% of GUA after 80 min of illumination. The increase in degradation efficiency of GUA was due to the formation of Fe(III)-oxalate complexes that were photolyzed to yield oxalate radicals (C₂O₄ $^{\bullet}$) triggering $^{\bullet}$ OH formation in the presence of dissolved oxygen (reaction 3, 5-9). Thus, increasing the concentration of oxalate enhances the yield of $^{\bullet}$ OH and concomitantly the degradation efficiency of GUA.

The initial photooxidation rate of GUA depended on the oxalate/Fe(III) molar ratio as well, although not monotonically. As shown in Figure S5, the GUA photooxidation followed pseudo-first order kinetics during the first 30 min of illumination and the rate increased with the oxalate/Fe(III) molar ratio between 1 to 9 but decreased from 9 to 12.5. This can be explained by the dependence of the speciation of Fe(III) complexes on oxalate concentration. As shown in Figure S6, at lower oxalate/Fe(III) molar ratio (e.g., 1:1), Fe(III) is mainly present as $[Fe(C_2O_4)]^+$ and $[Fe(OH)]^{2+}$, but the major Fe(III) complexes shift to $[Fe(C_2O_4)_2]^-$ and $[Fe(C_2O_4)_3]^{3-}$ at a high oxalate/Fe(III) molar ratio of 9. Since $[Fe(C_2O_4)_2]^-$ and $[Fe(C_2O_4)_3]^{3-}$ are much more photoactive than $[Fe(C_2O_4)]^+$ and $[Fe(OH)]^{2+}$, the formation rate of \cdot OH, and therefore the photooxidation rate of GUA, becomes faster

at higher oxalate concentration. But a lower initial degradation rate of GUA at oxalate concentration of 250 μ M compared to 180 μ M (Figure S5) suggests that excess oxalate inhibits the degradation of GUA initially. The reason may be that oxalate can also act as a scavenger of •OH produced in the Fenton reaction (reaction 3 or 9) and hence competes with GUA for •OH and significantly inhibits the degradation of GUA at high oxalate concentration.⁹ However, such inhibition effect declines with the consumption of oxalate.

289290

291

292

293

294

295

296

297

298

299

300

301

302303

304

305

306

307

308

309

310

311

312

313

314

315

282

283

284

285

286

287

288

3.2.3. Effects of Fe(III) concentration on the Fe(III)-oxalate mediated photooxidation of GUA

To investigate the effect of Fe(III) concentration on the photooxidation of GUA, solutions at pH 3.0 containing 5-30 µM Fe(III), 250 µM oxalate, and 50 µM GUA were irradiated with simulated sunlight. Figure 3b shows the time-variation of the concentration of GUA at different Fe(III) concentration. The photooxidation rate of GUA increased with Fe(III) concentration from 5 to 30 µM during the first 30 min of reaction and the pseudo-first order photooxidation rate constant of GUA increased from 0.008 to 0.041 min⁻¹ (Figure S7). Since a single Fe(III) ion can complex a number of oxalate ligand in the solution and oxalate was used in excess to Fe(III) in our experiments, increasing Fe(III) concentration enhances the concentration of Fe(III)-oxalate complexes, which leads to a higher H₂O₂ and Fe(II) concentrations due to ferrioxalate photolysis and concomitantly a higher 'OH concentration resulting from the Fenton reaction. However, when the reaction lasted for more than 1 hour, the most effective degradation was achieved at a Fe(III) concentration of 10 µM rather than 30 µM (Figure 3b). The difference between the red curve (10 µM) and the green curve (30 µM) at 80 min was statistically significant, which was unlikely the outcome of experimental errors (<2%). The reason may be that the competition reactions occurred between ferrioxalate and dissolved O₂ for CO₂ when Fe(III) concentration was relative high. At low concentration of ferrioxalate, CO2 mainly reacted with dissolved O2, contributing to the formation of H2O2 and OH, whereas at high concentration of ferrioxalate, a majority of CO₂ interacted with ferrioxalate, resulting in the formation of Fe(II) and CO₂ (reaction 12).³⁵ Thus, with the increase in Fe(III) concentration, more CO₂ would reduce Fe(III) to Fe(II) rather than react with O₂ to form H₂O₂, which leads to a decrease in •OH yield and degradation efficiency of GUA.

$[Fe(III)(C_2O_4)_3]^{3-} + CO_2^{\bullet-} \rightarrow [Fe(II)(C_2O_4)_2]^{2-} + CO_2 + C_2O_4^{2-}$ (12)

317

318

319

320

321

322

323

324

325

326

327

328

329

330

331

332

333

334

335

336

337

338

339

340

341

342

343

344

345

346

347

348

316

3.2.4. Effects of solution pH on the Fe(III)-oxalate mediated photooxidation of GUA

The solution pH has a profound effect on the speciation and reactivity of iron-catalyzed oxidative processes. The pH value in acidic atmospheric water typically ranges from 3 to 5.13 Therefore, experiments were carried out on the air-bubbled solution containing 20 µM Fe(III), 250 µM oxalate, and 50 µM GUA ³³with the pH adjusted from 3 to 5 to test the effects of pH on the photooxidation of GUA under simulated sunlight irradiation. As shown in Figure 3c, the photooxidation rate of GUA increased with increasing pH between 3.0 and 5.0. Besides, the photooxidation of GUA at different pH values followed pseudo-first order reaction and the rate constants increased from 0.026 to 0.099 min⁻¹ with the increase of pH value from 3 to 5 (Figure S8). The pH-dependence of GUA degradation in the photo/ferrioxalate system can be explained by the dependence of Fe(II) speciation on pH value, which affects the rate of the Fenton reaction. Free Fe(II) ions, the dominant Fe(II) species at low pH, reacts with H₂O₂ at a rate constant of 76 M⁻¹s⁻¹ (Reaction c in Table 1). With the increase of solution pH, the concentration of [Fe(II)(C₂O₄)] increases and [Fe(II)(C₂O₄)] is oxidized by H_2O_2 at a rate constant of $3.1 \times 10^4 \, M^{-1} s^{-1}$ (Reaction d in Table 1). Thus, the Fenton reaction is much faster at higher pH value. Furthermore, pH affects the reactions of active intermediates O₂•-/HO₂• with Fe(II), which represent a main source of H₂O₂ in Fe(III)-oxalate system. Thus, pH value has an important effect on the formation of H₂O₂. In addition, there are several competitive reactions of O₂•-/HO₂• with iron species (Reactions e-h listed in Table 1). Among them, the reactions between free Fe(III) ions and O₂•-/HO₂• could be ignored in spite of their high rate constants, since a tenfold (molar) excess of oxalate/Fe(III) used in this study ensured that almost all of Fe(III) presented as Fe(III)-oxalate complexes rather than free Fe(III) ions. Besides, the reactions between Fe(III)-oxalate complexes and O₂•-/HO₂• also became negligible as the photo-reduction of Fe(III)– oxalate complexes took place at much faster rates than the reduction of the Fe(III)oxalate complexes by $O_2^{\bullet-}/HO_2^{\bullet}$. Thus, the formation of H_2O_2 was mainly governed by the reactions of O2*-/HO2* with Fe(II). In the lower pH range, HO2* was the dominant species, while with the increase of pH value, O2 became more important. 13 The production of H₂O₂ through the Fe(II) + O₂ reaction is nearly an order of magnitude faster than that through the $Fe(II) + HO_2$ reaction (Reactions a and b in Table 1). Therefore, the increase in pH value led to faster OH generation and concomitantly greater GUA degradation.

Table 1. Reactions and reaction rate constants for Fe(II)/Fe(III) with $HO_2 \cdot /O_2 \cdot^-$ and H_2O_2 in aqueous phase.

No.	Reaction	$k (M^{-1} s^{-1})$	Ref.
a	$Fe(II) + HO_2 \cdot + H^+ \rightarrow Fe(III) + H_2O_2$	1.2×10^{6}	18
b	$Fe(II) + O_2^{\bullet-} + H^+ \rightarrow Fe(III) + H_2O_2$	1.0×10^7	18
c	$Fe(II) + H_2O_2 \rightarrow Fe(III) + OH \cdot + OH^-$	76	10
d	$[Fe(II)C_2O_4] + H_2O_2 \rightarrow [Fe(III)C_2O_4]^+ + OH^-$	3.1×10^{4}	19
e	$Fe(III) + HO_2 \cdot \longrightarrow Fe(II) + O_2 + H^+$	$< 1 \times 10^4$	18
f	$Fe(III) + O_2 \xrightarrow{\leftarrow} Fe(II) + O_2$	1.5×10^8	18
g	$[Fe(III)(C_2O_4)_n]^{3-2n} + HO_2 \cdot \longrightarrow [Fe(II)(C_2O_4)_n]^{2-2n} + O_2 + H^+$	$< 1.2 \times 10^5$	19
h	$[Fe(III)(C_2O_4)_n]^{3-2n} + O_2^{\bullet -} \rightarrow [Fe(II)(C_2O_4)_n]^{2-2n} + O_2$	$< 1 \times 10^6$	19
i	$Fe(III) + H_2O_2 \rightarrow Fe(II) + O_2 + H^+$	Very slow	10

3.2.5. Effects of the presence of oxygen on the Fe(III)-oxalate mediated photooxidation of GUA

In order to determine the effect of dissolved oxygen on the Fe-catalyzed photooxidation of GUA, photochemical experiments were conducted on the air- or nitrogen-saturated solutions containing 20 μ M Fe(III), 250 μ M oxalate, and 50 μ M GUA at pH 3.0. As shown in Figure 3d, only a slight decrease of GUA concentration was observed in the solution saturated with nitrogen after 100 min of simulated sunlight irradiation, which suggests the Fenton reaction pathways were inactive. In contrast, the concentration of GUA decreased significantly in the presence of air, which means that the oxidation of GUA in the irradiated ferrioxalate system needs the participation of oxygen. In addition, as shown in Figure S9, the concentration of H₂O₂ in the air-saturated solution increased continuously during the first 50 min then dropped off from 50 min to 100 min whereas H₂O₂ was below the detection limit (< 0.1 μ M) in the N₂-saturated solution during the entire experiment. These results stress the necessity of oxygen for the generation of H₂O₂ and •OH by photodissociation of Fe(III)-oxalate complexes.

The photolysis of Fe(III)-oxalate complex resulted in the reduction of Fe(III) to

Fe(II) and the formation of CO₂·-, which is a powerful reducing agent and could reduce another Fe(III)-oxalate ion or the dissolved O₂ depending on the relative concentrations of ferrioxalate to oxygen in the solution.³⁵ In air-saturated solution, the concentration of dissolved O₂ was about 250 μM, much higher than the 20 μM Fe(III) ion used in this study, thus CO₂·- would preferentially reduce O₂ to O₂·- rather than react with ferrioxalate to produce Fe(II).²⁵ The O₂·- and its conjugate acid (i.e., HO₂·) mainly reacted with Fe(II) to form H₂O₂ (reaction 8), which subsequently interacted with Fe(II) (reaction 3) or [Fe(II)C₂O₄] (reaction 9) to produce ·OH. In the absence of oxygen, CO₂·- can also react with GUA,³⁶ which explains the slight decline of GUA in the N₂-bubbling experiment (Figure 3d).

3.3. The photooxidation pathways of GUA in the presence of Fe(III)-oxalate complexes

Based on the molecular information obtained through the Orbitrap HRMS analysis, we elucidate the photooxidation mechanisms of GUA in Fe(III)-oxalate mediated systems. In the irradiated Fe(III)-oxalate system, attack by •OH was the predominant pathway for GUA degradation, while the other reactive oxygen species (e.g., O2•-/HO2•, H2O2) generated played an insignificant role in GUA degradation due to their lower reactivity towards phenols.³⁷ Previous studies have demonstrated that •OH plays a vital role in the transformation of dissolved organic pollutants in atmospheric water.^{2, 38} In general, •OH reacts with aromatic compounds via three channels: electron transfer, hydrogen atom abstraction and electrophilic addition. These reactions result in the substantial formation of low-volatility materials from GUA. For phenolic compounds such as GUA, electrophilic addition of •OH to the aromatic ring usually prevails over the other two channels.^{36, 39} H-abstraction from phenolic hydroxyl groups and methoxy groups is typically slow and H-abstraction from the aromatic ring is always a very minor reaction pathway. Electron transfer is a less common pathway because it requires very electron-rich matrices.³⁹⁻⁴¹

Figure 4 shows the Orbitrap mass spectra of the oxidative products formed in the GUA-Fe-oxalate solution after irradiation for 100 min. Note that a majority of the smaller and more oxidized ring-opening products are not included in Figure 4 as the mass spectra were acquired only for the range of m/z 90-500. The Van Krevelen diagram (Figure S10) reveals the presence of a large number of molecules with double bond equivalent (DBE) > 5, suggesting that they contain at least one aromatic

ring. Table S1 lists 40 key molecules identified as the products of GUA photooxidation, including hydroxylated species, aldehydes, acids, esters, oligomers, epoxide, hydroperoxide and quinone. For example, the ions at m/z = 139.03976 $(C_7H_7O_3^-)$ and m/z = 261.07693 $(C_{14}H_{13}O_5^-)$ suggested the presence of hydroxylated GUA and hydroxylated GUA dimer, respectively. Poly-hydroxylated products were also identified, as the ions at $m/z = 171.02946 \, (\text{C}_7\text{H}_7\text{O}_5^-)$ and m/z = 187.02462(C₇H₇O₆⁻) were assigned to the low-volatility products, i.e., trihydroxy and tetrahydroxy guaiacol, respectively. These results indicate that hydroxylation was a significant reaction pathway that led to the oxidation of GUA. Oligomerization was another reaction channel that contributed to the transformation of GUA (Table S1). The high abundance of ions at m/z = 245.08215 (C₁₄H₁₃O₄⁻) and m/z = 243.06636(C₁₄H₁₁O₄⁻) in the HRMS indicates the presence of guaiacol dimer and its derivative (Figure 5, A₁₆, A₁₇, A₁₈). However, ions representing trimer and higher oligomer were not detected at significant signal-to-noise ratios in the HRMS, implying that the products were highly oxygenated in the irradiated Fe(III)-oxalate system. According to the study of Yu et al., 42 the GUA oligomers are intermediate products mainly formed in the initial stage of OH- mediated reactions. As the reaction proceeds, longer aging can lead to the fragmentation of oligomers, forming more oxygenated and smaller products. 42

407

408

409

410

411

412

413

414

415

416

417

418

419

420

421

422

423

424

425

426

427

428

429

430

431

432

433

434

435

436

437

438

439

440

The HRMS results revealed the ubiquitous formation of acid, esters, epoxide, hydroperoxide, quinone from GUA as well. For example, the noticeable peaks at m/z= 179.03482 (C₉H₇O₄⁻) and m/z = 195.02994 (C₉H₇O₅⁻) in the HRMS of the products suggested the formation of two kinds of guaiacol esters, 2-methoxy phenyl glyoxylate and 2-methoxy phenyl oxalate. The peak at m/z = 205.03497 ($C_7H_9O_7^-$) implied the presence of highly oxidized species bicyclic hydroperoxide (Figure 5, A₆). The pronounced signal at m/z=123.00863 $(C_6H_3O_3^-)$ was assigned hydroxybenzoquinone, which was likely a demethoxylated aromatic product of GUA oxidation. Interestingly, demethoxylation of GUA by OH also led to the formation of dihydroxybenzene (catechol), a marker for biomass burning, corresponding to the strong signal at m/z = 109.02923 (C₆H₅O₂⁻). The peak at m/z = 171.02946 (C₇H₇O₅⁻) represented a ring-cleavage epoxy product of GUA oxidation (Figure 6, B₅). Besides, a large number of low-molecular-weight products (number of C atoms <6), such as $C_4H_3O_4$ at m/z = 115.00338 and $C_5H_5O_4$ at m/z = 129.01919, were identified. These small organic acids were highly oxygenated open-ring products of GUA.

441 Based on the above results, we proposed in Figure 5 the main pathways of GUA oxidation through the reactions with OH. Briefly, the reactions with organic 442 acids can lead to the esterification of GUA.⁴³ For example, the reaction between GUA 443 and oxalic acid produces a phenolic ester – methoxyphenyl oxalate (A₁). 444 H-abstraction from the methoxy group of GUA by OH, followed by OH addition to 445 OCH₂ radical group, results in the formation of a hemiacetal (A₂), which is a minor 446 route for GUA oxidation by 'OH.44 The electrophilic ortho-addition of 'OH to the 447 aromatic ring of GUA, followed by O₂ addition, leads to the formation of the primary 448 449 peroxy radical (A₃), which can react with HO₂ to form guaiacol hydroperoxide (A₄). The primary peroxy radical (A₃) can also isomerize to form bicyclic peroxy radical 450 (A₅), which will proceed through H-abstraction from HO₂ to form bicyclic 451 hydroperoxide (A₆). The *ortho*-addition of •OH to the ring, followed by O₂ addition 452 and HO_2 the elimination, results in formation of 453 2-hydroxy-6-methoxy-3,5-cyclohexadienone (A₇) and monohydroxy guaiacol (A₈). A₈ 454 can be further oxidized to form 2-methoxy-o-quinone (A₉) through H-abstraction 455 from hydroxyl groups by OH, O2 addition, then HO2 elimination. In addition, 456 H-abstraction from phenolic hydroxyl groups of GUA by OH leads to the formation 457 of phenoxy radical, which is known to undergo radical recombination via C-C or C-O 458 coupling in aqueous phase to form dimers (A₁₆, A₁₇ and A₁₈).⁴⁵ Demethoxylation 459 occurs through electrophilic ipso-addition of 'OH to ring positions occupied by 460 methoxyl groups, followed by elimination of a methanol molecule to yield 461 semiquinone radicals (A₁₀).⁴⁶ A₁₀ can directly interact with HO₂ to form 462 dihydroxybenzene $(A_{15})^{44,47}$ or isomerize to form alkyl radical (A_{11}) . A_{11} reacts 463 rapidly with O₂ to yield peroxy radical (A₁₂), which is then reduced to alkoxy radical 464 (A₁₃) by HO₂. A₁₃ will further undergo H-abstraction by O₂ to yield 465 2-hydroxy-p-benzoguinone (A₁₄). This demethoxy route eventually leads to carbon 466 loss from methoxyphenol system and converts methoxy groups to hydroxyl or 467 carbonyl groups. To further confirmed the occurrence of the methoxy loss route, we 468 employed GC-MS to identify methanol in the photooxidation products of GUA and 469 unambiguously detected methanol in the products (Figure S11). According to the 470 study of Aihara et al. 44, ipso-addition of OH is a more important route compared to 471 ortho- and para-addition of OH to the ring of methoxyphenol in aqueous phase, so 472 ipso-addition of OH may be a major route that leads to the oxidation of GUA in 473 current systems. 474

Furthermore, the reactants and products from all these reaction pathways can further undergo ring opening and fragmentation processes, resulting in the substantial formation of aldehyde, ketone, epoxide and carboxylic acid. Since almost all low-volatility small molecules (C number <6) in the oxidative products of aromatics originate from the open-ring processes, the ring-opening reactions initiated by 'OH play a significant role in producing aromatic SOA in both gas phase and liquid phase. The OH-mediated ring-opening oxidation mechanisms for gas-phase aromatic organics have been investigated extensively, but very little is known for the liquid-phase reactions of aromatics. Figure 6 shows the ring-opening oxidative mechanisms of GUA mediated by 'OH in water. The addition of 'OH and O2 to the aromatic ring of GUA leads to the formation of primary peroxy radical (B₁), which would preferably cyclize to the bicyclic allyl radical (B2) since the allylically stabilized five-membered bicyclic radicals are the lowest energy radicals formed. 48, 49 The bicyclic intermediate B₂ is the source for the reaction pathways that lead to the formation of ring-opening products.⁵⁰ B₂ will go on to react via two channels. One channel is to break the -O-O- bond of B₂ to form epoxy alkoxy radicals (B₃). The breakage of the aromatic ring on B₃ produces epoxide-containing radical product (B₄), which undergoes H-abstraction by O₂ to yield the unsaturated epoxy-1,6-dicarbonyl (B₅) eventually.⁵¹ In the other channel, B₂ combines with O₂ to produce bicyclic peroxy radical (B₆), which is reduced to a bicyclic alkoxy radical (B₇) by HO₂. B₇ subsequently undergoes two contrary processes: ring-breakage or ring-closure. The β-scission of B₇ gives the ring-open radical product (B₈), which breaks the -O-Obond to form a radical (B₉). B₉ then decomposes via the C-C scission to ultimately form glyoxal and highly oxygenated unsaturated carboxylic acid (B₁₀). It is important to note that the scission occurs preferably at the C-C bond between the carbon with the oxygen atom attached to it and the saturated carbon center.⁴⁹ The ring-closure of B₇ produces bicyclic epoxyl radical (B₁₁), which then recombines with O₂ to form bicyclic epoxyl peroxy radical (B₁₂). B₁₂ would react with HO₂ to form bicyclic epoxyl alkoxy radical (B₁₃), which is subject to C-C bond breakages and to H-abstraction by O₂ to eventually yield glyoxylic acid and highly oxidized epoxy-1,4-dicarbonyl (B₁₄).⁵² These results reveal that OH-mediated ring-opening reactions of GUA in liquid phase may be a significant source of small-molecular products such as glyoxal, glyoxylic acid as well as highly oxidized species in the atmosphere. Note that the ring-opening mechanisms mediated by 'OH are also

475

476

477

478

479

480

481

482

483

484

485

486

487

488

489

490

491

492

493

494

495 496

497

498

499

500

501

502

503

504

505

506

507

applicable to other oxidized products containing aromatic ring in current reaction system.

4. Environmental significance

We studied the importance of Fe and oxalate in the aqueous aging of GUA. For the dark reaction, the presence of oxalate inhibits the Fe(III)-oxidation of GUA. For the photoreaction, the presence of oxalate can strongly promote the Fe-catalyzed oxidation of GUA via the formation of photoactive Fe(III)-oxalate complexes which can undergo efficient photodissociation to produce 'OH under simulated sunlight. The photodegradation rate and efficiency of GUA increase with the increase of pH value from 3 to 5. By using high resolution mass spectrometry, a large number of products with different degrees of oxidation (including dimers and their related derivatives, ring-opening products, functionalized products) were identified. The reaction mechanism is proposed in detail based on the molecular analysis by HRMS.

It is expected that the formation of oxidants in atmospheric water by photolysis of Fe(III)-oxalate complexes is continuous since oxalate are continuously replenished by gas-to-liquid partitioning and in-cloud oxidation of other organic matters. In addition to oxalate, other organic acids in atmospheric water such as pyruvate and glyoxalate can form complexes with Fe(III) and these Fe(III)-organic complexes have been reported to generate reactive oxidative species such as •OH and H₂O₂.^{13, 53} Although we only focused on the role that the Fe(III)-oxalate complexes play in the chemical evolution of GUA, other Fe(III)-organic complexes may also play a significant role in the degradation of GUA and other soluble organics in atmospheric aqueous phase. Therefore, our work implies that the Fe(III)-organic complexes are potentially a powerful source of oxidants in atmospheric condensed phases and play a significant role in the transformation of the dissolved organic compounds in the atmosphere.

Supporting information

Materials and reagents, additional experimental details, analytical procedures, Figure S1-S11 and Table S1.

Acknowledgements

This work was supported by the National Natural Science Foundation of China

- 543 (Nos. 91544224, 21507010, 41775150, 41827804). QZ also acknowledges the
- funding from the National Science Foundation grant number AGS- 1649212.

References

- 547 (1) Deguillaume, L.; Leriche, M.; Desboeufs, K.; Mailhot, G.; George, C.; Chaumerliac, N. Transition
- metals in atmospheric liquid phases: Sources, reactivity, and sensitive parameters. Chem. Rev. 2005,
- 549 *105* (9), 3388-3431.
- 550 (2) Herrmann, H.; Schaefer, T.; Tilgner, A.; Styler, S. A.; Weller, C.; Teich, M.; Otto, T. Tropospheric
- 551 aqueous-phase chemistry: kinetics, mechanisms, and its coupling to a changing gas phase. Chem. Rev.
- **2015,** *115* (10), 4259-4334.
- 553 (3) Al-Abadleh, H., Review on the Bulk and Surface Chemistry of Iron in Atmospherically-Relevant
- 554 Systems Containing Humic like Substances. RSC Advance, 5, 45785-45811. In 2015.
- 555 (4) Deng, Y.; Zhang, K.; Chen, H.; Wu, T.; Krzyaniak, M.; Wellons, A.; Bolla, D.; Douglas, K.; Zuo,
- 556 Y. Iron-catalyzed photochemical transformation of benzoic acid in atmospheric liquids: Product
- 557 identification and reaction mechanisms. Atmos. Environ. Part B 2006, 40 (20), 3665-3676.
- 558 (5) Slikboer, S.; Grandy, L.; Blair, S. L.; Nizkorodov, S. A.; Smith, R. W.; Al-Abadleh, H. A.
- Formation of light absorbing soluble secondary organics and insoluble polymeric particles from the
- dark reaction of catechol and guaiacol with Fe (III). Environ. Sci. Technol. 2015, 49 (13), 7793-7801.
- 561 (6) Moonshine, M.; Rudich, Y.; Katsman, S.; Graber, E. Atmospheric HULIS enhance pollutant
- degradation by promoting the dark Fenton reaction. *Geophys. Res. Lett.* **2008**, *35* (20), L20807.
- 563 (7) Nguyen, T.; Coggon, M.; Flagan, R.; Seinfeld, J. Reactive uptake and photo-fenton oxidation of
- glycolaldehyde in aerosol liquid water. *Environ. Sci. Technol.* **2013**, *47* (9), 4307-4316.
- 565 (8) Feng, W.; Nansheng, D. Photochemistry of hydrolytic iron (III) species and photoinduced
- degradation of organic compounds. A minireview. *Chemosphere* **2000**, *41* (8), 1137-1147.
- 567 (9) Balmer, M. E.; Sulzberger, B. Atrazine degradation in irradiated iron/oxalate systems: effects of
- 568 pH and oxalate. *Environ. Sci. Technol.* **1999**, *33* (14), 2418-2424.
- 569 (10) Walling, C. Fenton's reagent revisited. Acc. Chem. Res. 1975, 8 (4), 125-131.
- 570 (11) Thomas, D. A.; Coggon, M. M.; Lignell, H.; Schilling, K. A.; Zhang, X.; Schwantes, R. H.;
- 571 Flagan, R. C.; Seinfeld, J. H.; Beauchamp, J. L. Real-Time Studies of Iron Oxalate-Mediated Oxidation
- 572 of Glycolaldehyde as a Model for Photochemical Aging of Aqueous Tropospheric Aerosols. *Environ*.
- 573 Sci. Technol. 2016, 50 (22), 12241-12249.
- 574 (12) Weller, C.; Horn, S.; Herrmann, H. Photolysis of Fe (III) carboxylato complexes: Fe (II) quantum
- 575 yields and reaction mechanisms. J. Photochem. Photobiol., A 2013, 268, 24-36.
- 576 (13) Zuo, Y.; Hoigne, J. Formation of hydrogen peroxide and depletion of oxalic acid in atmospheric
- water by photolysis of iron (III)-oxalato complexes. *Environ. Sci. Technol.* **1992**, *26* (5), 1014-1022.
- 578 (14) Zuo, Y. Kinetics of photochemical/chemical cycling of iron coupled with organic substances in
- 579 cloud and fog droplets. *Geochim. Cosmochim. Acta* **1995,** *59* (15), 3123-3130.
- 580 (15) Mangiante, D. M.; Schaller, R. D.; Zarzycki, P.; Banfield, J. F.; Gilbert, B. Mechanism of Ferric
- Oxalate Photolysis. ACS Earth and Space Chemistry 2017, 1 (5), 270-276.
- 582 (16) Mulazzani, Q. G.; D'Angelantonio, M.; Venturi, M.; Hoffman, M. Z.; Rodgers, M. A. Interaction
- 583 of formate and oxalate ions with radiation-generated radicals in aqueous solution. Methylviologen as a
- mechanistic probe. *J. Phys. Chem.* **1986**, *90* (21), 5347-5352.
- 585 (17) Weller, C.; Horn, S.; Herrmann, H. Effects of Fe (III)-concentration, speciation,
- excitation-wavelength and light intensity on the quantum yield of iron (III)-oxalato complex photolysis.

- 587 *J. Photochem. Photobiol., A* **2013,** *255*, 41-49.
- 588 (18) Rush, J. D.; Bielski, B. H. Pulse radiolytic studies of the reactions of HO2/O2 with Fe (II)/Fe (III)
- 589 ions. The reactivity of HO2/O2 with ferric ions and its implication on the occurrence of the
- 590 Haber-Weiss reaction. J. Phys. Chem. 1985, 89 (23), 5062-5066.
- 591 (19) Sedlak, D. L.; Hoigné, J. The role of copper and oxalate in the redox cycling of iron in
- 592 atmospheric waters. Atmospheric Environment. Part A. General Topics 1993, 27 (14), 2173-2185.
- 593 (20) Wang, Z.; Xiao, D.; Liu, J. Diverse redox chemistry of photo/ferrioxalate system. RSC Adv. 2014,
- 594 *4* (84), 44654-44658.
- 595 (21) Jeong, J.; Yoon, J. pH effect on OH radical production in photo/ferrioxalate system. Water Res.
- **2005**, *39* (13), 2893-2900.
- 597 (22) Pozdnyakov, I. P.; Kel, O. V.; Plyusnin, V. F.; Grivin, V. P.; Bazhin, N. M. New insight into
- 598 photochemistry of ferrioxalate. J. Phys. Chem. A 2008, 112 (36), 8316-8322.
- 599 (23) Chen, J.; Zhang, H.; Tomov, I. V.; Rentzepis, P. M. Electron transfer mechanism and
- photochemistry of ferrioxalate induced by excitation in the charge transfer band. *Inorg. Chem.* 2008, 47
- 601 (6), 2024-2032.
- 602 (24) Wang, Z.; Chen, C.; Ma, W.; Zhao, J. Photochemical coupling of iron redox reactions and
- transformation of low-molecular-weight organic matter. J. Phys. Chem. Lett. 2012, 3 (15), 2044-2051.
- 604 (25) Zuo, Y.; Zhan, J. Effects of oxalate on Fe-catalyzed photooxidation of dissolved sulfur dioxide in
- atmospheric water. *Atmos. Environ. Part B* **2005**, *39* (1), 27-37.
- 606 (26) Schauer, J. J.; Kleeman, M. J.; Cass, G. R.; Simoneit, B. R. Measurement of emissions from air
- 607 pollution sources. 3. C1- C29 organic compounds from fireplace combustion of wood. *Environ. Sci.*
- 608 Technol. 2001, 35 (9), 1716-1728.
- 609 (27) Murov, S. L.; Carmichael, I.; Hug, G. L., Handbook of photochemistry. CRC Press: 1993.
- 610 (28) Zuo, Y. High-performance liquid chromatography (HPLC): principles, procedures and practices.
- 611 New York: Nova Science 2014.
- 612 (29) Lavi, A.; Lin, P.; Bhaduri, B.; Carmieli, R.; Laskin, A.; Rudich, Y. Characterization of
- 613 Light-Absorbing Oligomers from Reactions of Phenolic Compounds and Fe (III). ACS Earth and
- 614 Space Chemistry **2017**, 1 (10), 637-646.
- 615 (30) Rodríguez, E.; Mimbrero, M.; Masa, F. J.; Beltrán, F. J. Homogeneous iron-catalyzed
- photochemical degradation of muconic acid in water. Water Res. 2007, 41 (6), 1325-1333.
- 617 (31) Zhou, D.; Wu, F.; Deng, N.; Xiang, W. Photooxidation of bisphenol A (BPA) in water in the
- presence of ferric and carboxylate salts. *Water Res.* **2004**, *38* (19), 4107-4116.
- 619 (32) Zuo, Y. Light-induced formation of hydroxyl radicals in fog waters determined by an authentic
- 620 fog constituent, hydroxymethanesulfonate. *Chemosphere* **2003**, *51* (3), 175-179.
- 621 (33) Liu, G.; Zheng, S.; Xing, X.; Li, Y.; Yin, D.; Ding, Y.; Pang, W. Fe (III)-oxalate complexes
- 622 mediated photolysis of aqueous alkylphenol ethoxylates under simulated sunlight conditions.
- 623 Chemosphere **2010**, 78 (4), 402-408.
- 624 (34) Zepp, R. G.; Hoigne, J.; Bader, H. Nitrate-induced photooxidation of trace organic chemicals in
- 625 water. Environ. Sci. Technol. 1987, 21 (5), 443-450.
- 626 (35) Jeong, J.; Yoon, J. Dual roles of CO2- for degrading synthetic organic chemicals in the
- 627 photo/ferrioxalate system. *Water Res.* **2004,** *38* (16), 3531-3540.
- 628 (36) Zhao, C.; Arroyo-Mora, L. E.; DeCaprio, A. P.; Sharma, V. K.; Dionysiou, D. D.; O'Shea, K. E.
- Reductive and oxidative degradation of iopamidol, iodinated X-ray contrast media, by Fe (III)-oxalate
- under UV and visible light treatment. Water Res. 2014, 67, 144-153.

- 631 (37) Kozmér, Z.; Arany, E.; Alapi, T.; Takács, E.; Wojnárovits, L.; Dombi, A. Determination of the rate
- 632 constant of hydroperoxyl radical reaction with phenol. *Radiat. Phys. Chem.* 2014, 102, 135-138.
- 633 (38) Herrmann, H.; Hoffmann, D.; Schaefer, T.; Bräuer, P.; Tilgner, A. Tropospheric aqueous phase
- 634 free radical chemistry: Radical sources, spectra, reaction kinetics and prediction tools.
- 635 *ChemPhysChem* **2010**, *11* (18), 3796-3822.
- 636 (39) Gligorovski, S.; Strekowski, R.; Barbati, S.; Vione, D. Environmental implications of hydroxyl
- 637 radicals (• OH). Chem. Rev. 2015, 115 (24), 13051-13092.
- 638 (40) Sandhiya, L.; Kolandaivel, P.; Senthilkumar, K. Mechanism and Kinetics of the Atmospheric
- Oxidative Degradation of Dimethylphenol Isomers Initiated by OH Radical. J. Phys. Chem. A 2013,
- 640 117 (22), 4611-4626.
- 641 (41) Hoffmann, E. H.; Tilgner, A.; Wolke, R.; Böge, O.; Walter, A.; Herrmann, H. Oxidation of
- substituted aromatic hydrocarbons in the tropospheric aqueous phase: kinetic mechanism development
- and modelling. *PCCP* **2018**, *20* (16), 10960-10977.
- 644 (42) Yu, L.; Smith, J.; Laskin, A.; George, K. M.; Anastasio, C.; Laskin, J.; Dillner, A. M.; Zhang, Q.
- Molecular transformations of phenolic SOA during photochemical aging in the aqueous phase:
- competition among oligomerization, functionalization, and fragmentation. Atmos. Chem. Phys. 2016,
- 647 *16* (7), 4511-4527.
- 648 (43) Offenhauer, R. D. The direct esterification of phenols. J. Chem. Educ. 1964, 41 (1), 39.
- 649 (44) Aihara, K.; Urano, Y.; Higuchi, T.; Hirobe, M. Mechanistic studies of selective catechol formation
- 650 from o-methoxyphenols using a copper (II)-ascorbic acid-dioxygen system. J. Chem. Soc., Perkin
- 651 Trans. 2 1993, (11), 2165-2170.
- 652 (45) Sun, Y.; Zhang, Q.; Anastasio, C.; Sun, J. Insights into secondary organic aerosol formed via
- aqueous-phase reactions of phenolic compounds based on high resolution mass spectrometry. Atmos.
- 654 Chem. Phys. 2010, 10 (10), 4809-4822.
- 655 (46) Steenken, S.; O'Neill, P. Oxidative demethoxylation of methoxylated phenols and hydroxybenzoic
- acids by the hydroxyl radical. An in situ electron spin resonance, conductometric pulse radiolysis and
- 657 product analysis study. J. Phys. Chem. 1977, 81 (6), 505-508.
- 658 (47) Atkinson, R.; Lloyd, A. C. Evaluation of kinetic and mechanistic data for modeling of
- 659 photochemical smog. J. Phys. Chem. Ref. Data 1984, 13 (2), 315-444.
- 660 (48) Glowacki, D. R.; Wang, L.; Pilling, M. J. Evidence of formation of bicyclic species in the early
- stages of atmospheric benzene oxidation. *J. Phys. Chem. A* **2009**, *113* (18), 5385-5396.
- 662 (49) Andino, J. M.; Smith, J. N.; Flagan, R. C.; Goddard, W. A.; Seinfeld, J. H. Mechanism of
- atmospheric photooxidation of aromatics: A theoretical study. J. Phys. Chem. 1996, 100 (26),
- 664 10967-10980.
- 665 (50) Volkamer, R.; Platt, U.; Wirtz, K. Primary and secondary glyoxal formation from aromatics:
- experimental evidence for the bicycloalkyl- radical pathway from benzene, toluene, and p-xylene. J.
- 667 Phys. Chem. A 2001, 105 (33), 7865-7874.
- 668 (51) Wu, R.; Pan, S.; Li, Y.; Wang, L. Atmospheric oxidation mechanism of toluene. J. Phys. Chem. A
- **2014,** *118* (25), 4533-4547.
- 670 (52) Wang, L.; Wu, R.; Xu, C. Atmospheric oxidation mechanism of benzene. Fates of alkoxy radical
- intermediates and revised mechanism. *J. Phys. Chem. A* **2013**, *117* (51), 14163-14168.
- 672 (53) Zuo, Y.; Hoigné, J. Photochemical decomposition of oxalic, glyoxalic and pyruvic acid catalysed
- 673 by iron in atmospheric waters. *Atmos. Environ. Part B* **1994**, *28* (7), 1231-1239.

677 Figures

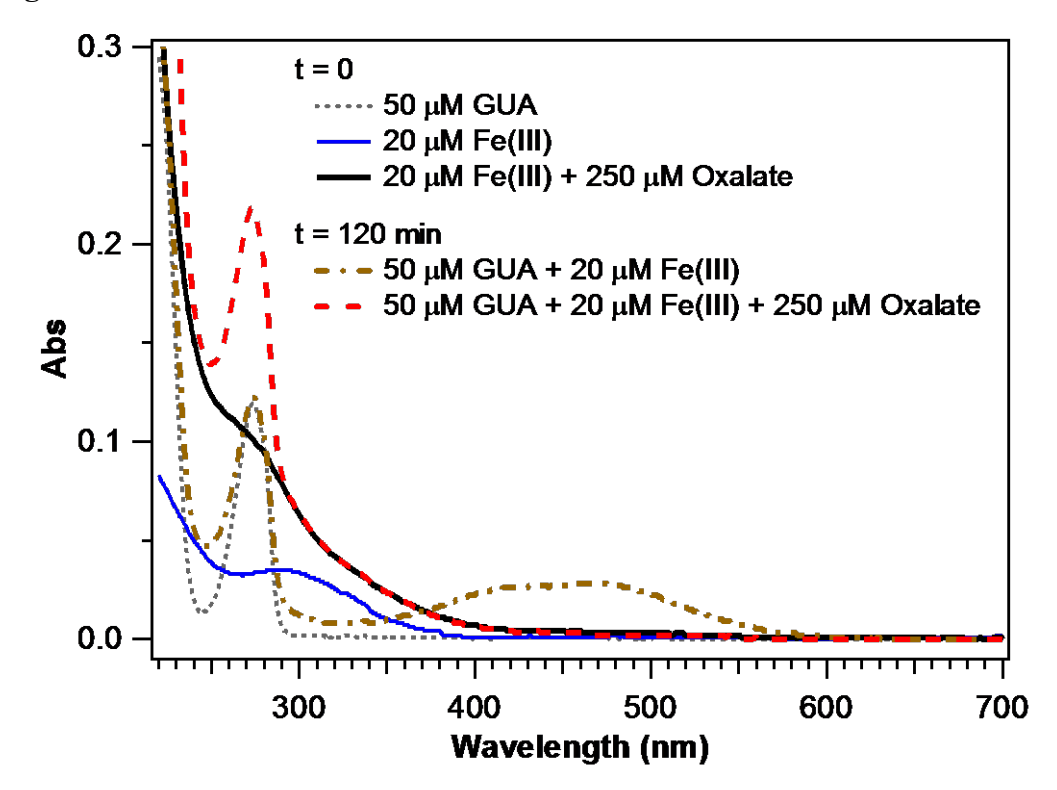


Figure 1. Comparison of UV-vis absorption spectra of solution containing 50 μM GUA, t=0; solution containing 20 μM Fe(III), t=0; solution containing 20 μM Fe(III) and 250 μM oxalate, t=0; solution containing 20 μM Fe(III) and 50 μM GUA, t=120 min; and solution containing 20 μM Fe(III), 250 μM oxalate and 50 M GUA, t=120 min at pH = 3.0 ± 0.1 in dark conditions.

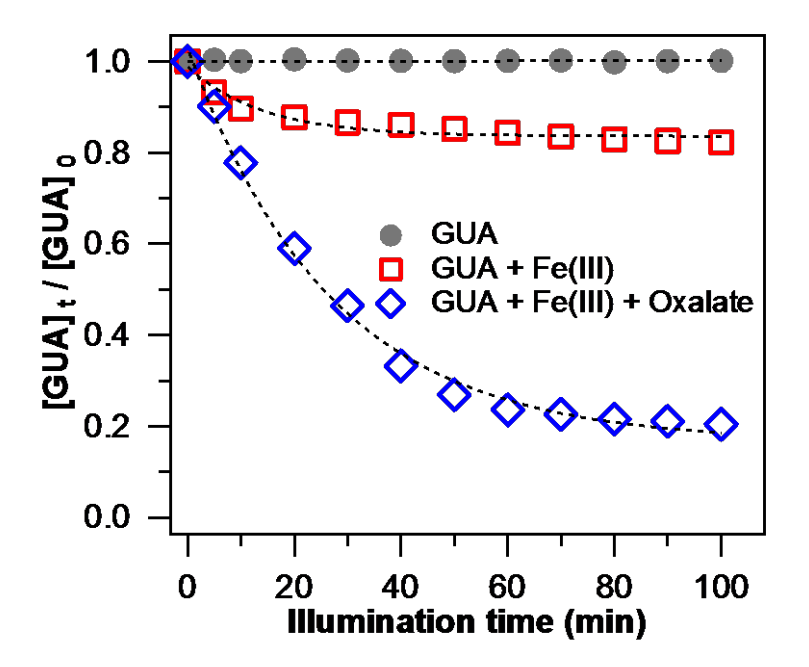


Figure 2. GUA concentration change vs time in the control experiments $[Fe(III)]_0 = 20 \mu M$, $[Oxalate]_0 = 250 \mu M$, $[GUA]_0 = 50 \mu M$, $pH = 3.0 \pm 0.1$, air saturated solution.

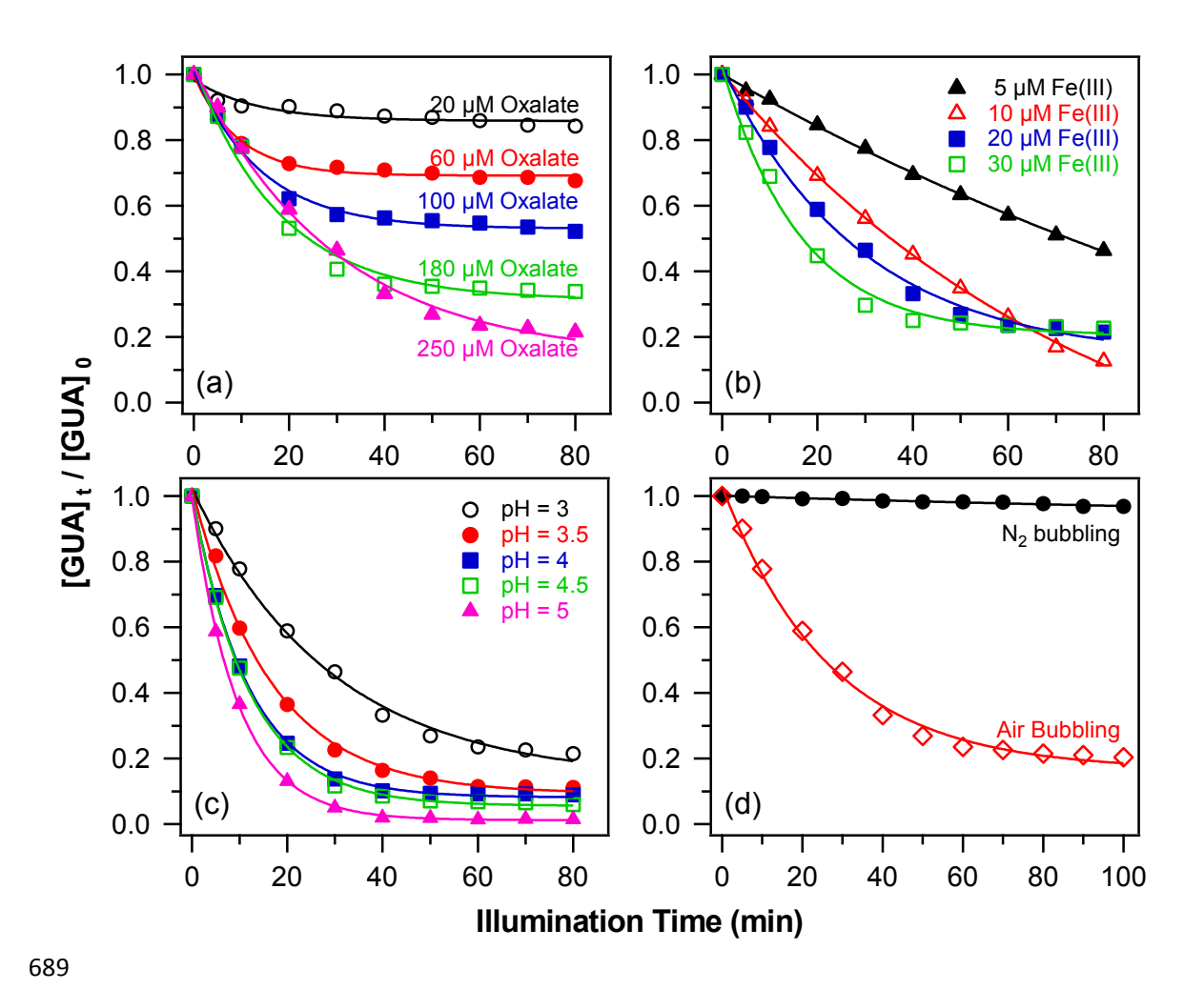


Figure 3. (a). Effect of oxalate concentration on the Fe(III)-oxalate mediated photooxidation of GUA. [Fe(III)]₀ = 20 μM, [GUA]₀ = 50 μM, pH = 3.0 ± 0.1 , air saturated solution; **(b).** Effect of Fe(III) concentration on the Fe(III)-oxalate mediated photooxidation of GUA. [Oxalate]₀ = 250 μM, [GUA]₀ = 50 μM, pH = 3.0 ± 0.1 , air saturated solution; **(c).** Effect of solution pH on the Fe(III)-oxalate mediated photooxidation of GUA. [Fe(III)]₀ = 20 μM, [Oxalate]₀ = 250 μM, [GUA]₀ = 50 μM, air saturated solution; **(d).** Effect of the presence of oxygen on the Fe(III)-oxalate mediated photooxidation of GUA. [Fe(III)]₀ = 20 μM, [Oxalate]₀ = 250 μM, [GUA]₀ = 50μ M, pH = 3.0 ± 0.1 , air bubbling, nitrogen bubbling.

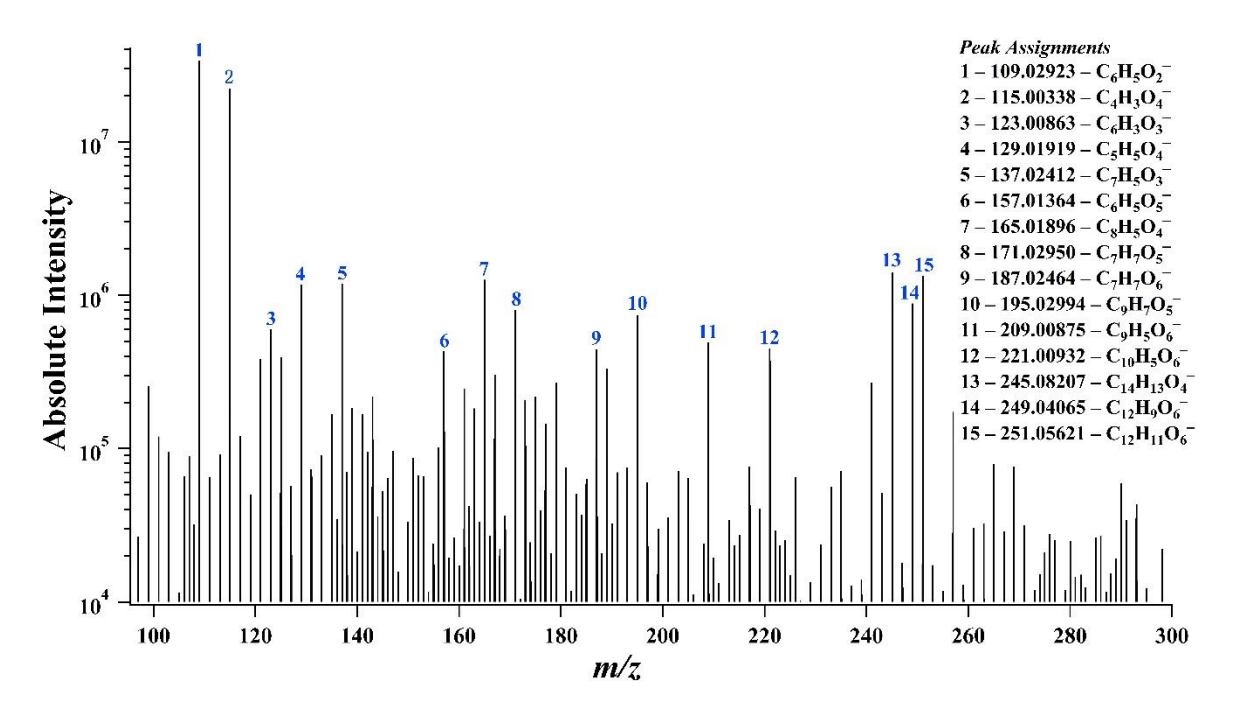


Figure 4. Orbitrap mass spectrum the oxidative products of GUA from the photo/ferrioxalate system: $[Fe(III)]_0 = 20 \mu M$, $[Oxalate]_0 = 250 \mu M$, $[GUA]_0 = 50 \mu M$, pH = 3.0 \pm 0.1, air bubbling. The mass spectrum was acquired in negative electrospray ionization modes. The proposed chemical structures for the compounds identified in Figure 4 are presented in Table S1 in the Supporting Information.

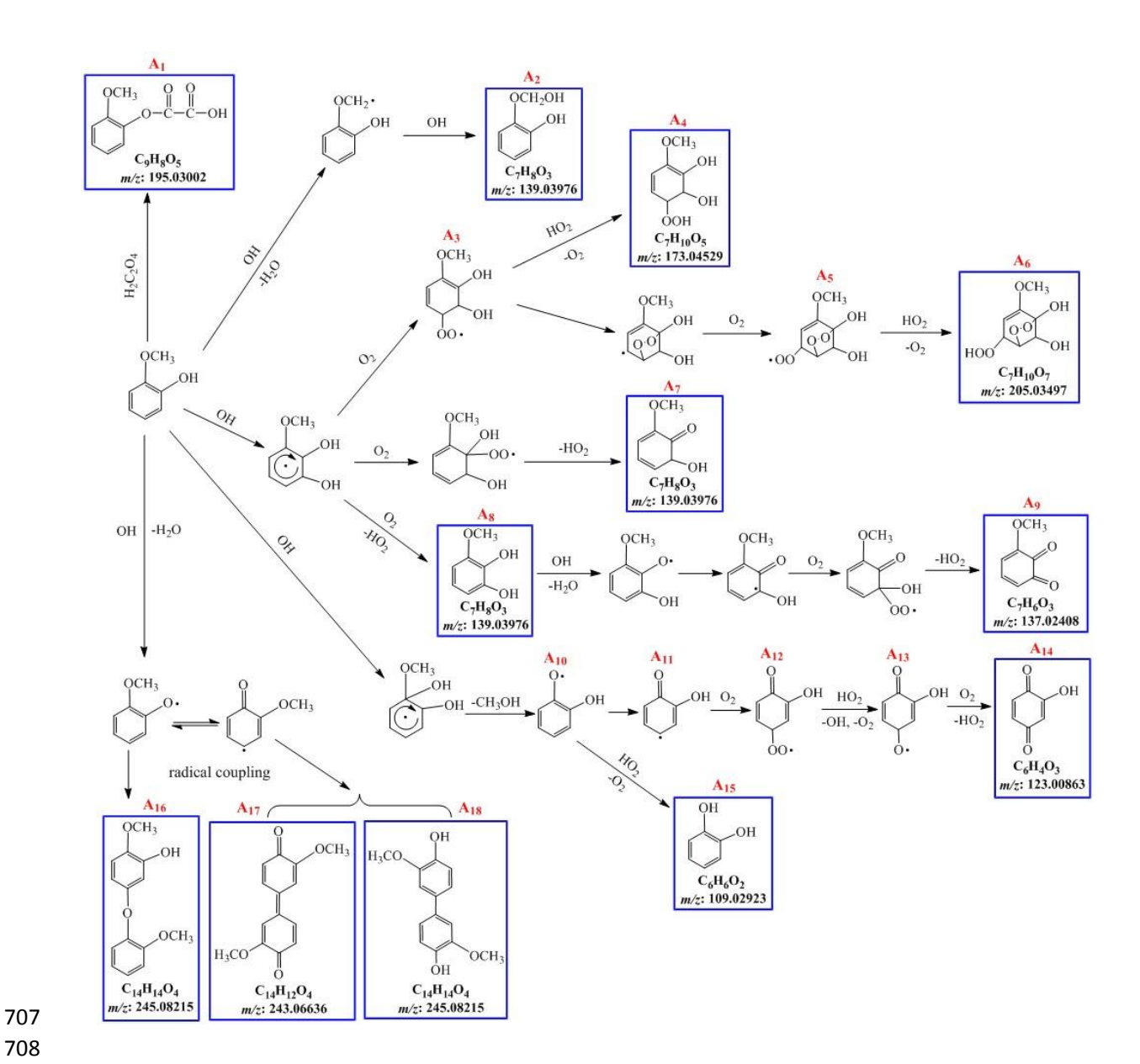


Figure 5. Proposed mechanisms for the formation of hydroxylated species, dimers esters, quinones, ketones, hydroperoxide and demethoxylated products from aqueous reactions of GUA with OH radical generated by the photolysis of Fe(III)-oxalate complexes. All the species produced via the reactions of GUA with OH may undergo further ring-opening processes to form ketones, aldehyde, epoxide and carboxylic acids. Compounds highlighted in blue boxes were detected by Orbitrap-MS.

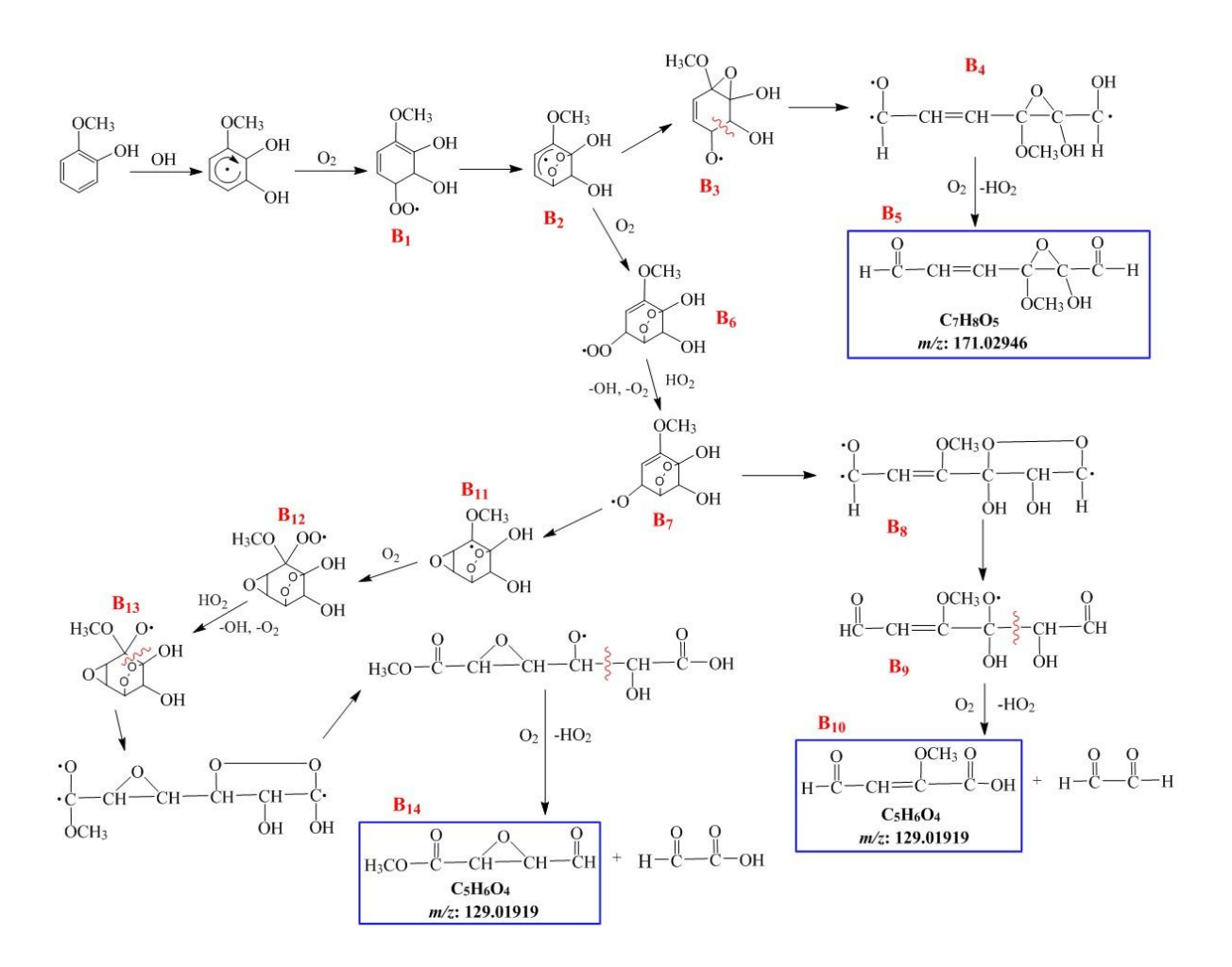
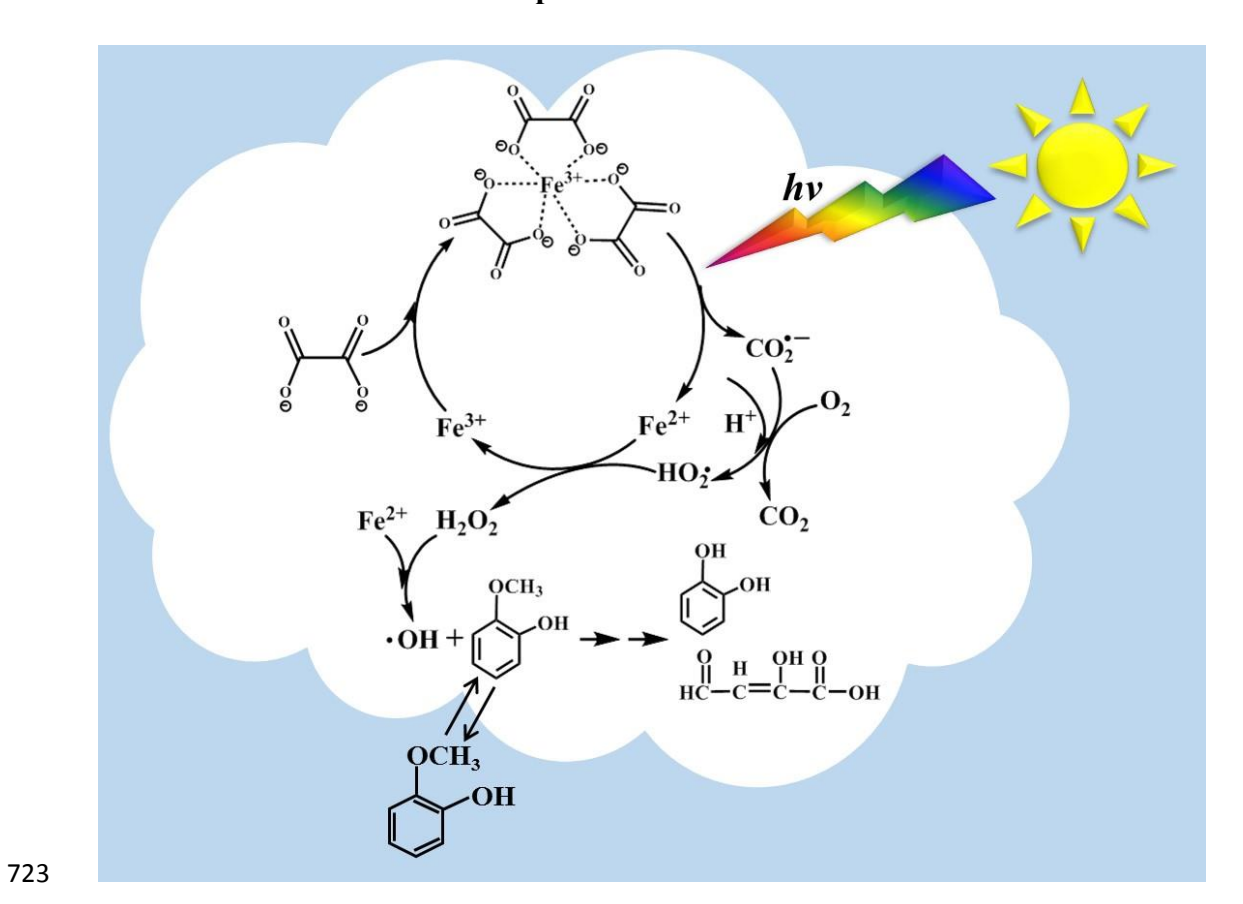


Figure 6. Proposed ring-opening mechanisms for the reaction of GUA with OH radical generated by the photolysis of Fe(III)-oxalate complexes. Compounds highlighted in blue boxes were detected by Orbitrap-MS.

722 Table of Contents/ Abstract Graphics



Supporting information

Photochemical aging of guaiacol by Fe(III)-oxalate complexes in atmospheric aqueous phase Hongwei Pang¹, Qi Zhang², Hongli Wang³, Dongmei Cai¹, Yingge Ma³, Li Li³, Kangning Li¹, Xiaohui Lu^{1*}, Hong Chen¹, Xin Yang^{1,4*}, Jianmin Chen¹ ¹Shanghai Key Laboratory of Atmospheric Particle Pollution and Prevention, Department of Environmental Science and Engineering, Fudan University, Shanghai 200433, China ²Department of Environmental Toxicology, University of California, Davis, California 95616, United States ³State Environmental Protection Key Laboratory of Formation and Prevention of the Urban Air Pollution Complex, Shanghai Academy of Environmental Sciences, Shanghai 200233, China ⁴Shanghai Institute of Pollution Control and Ecological Security, Shanghai 200092, China Correspondence to: Xiaohui Lu (luxiaohui@fudan.edu.cn); Xin Yang (yangxin@fudan.edu.cn)

41	Contents:
42	
43	Text S1. Materials and reagents · · · Page S3
44	Text S2. Additional experimental details · · · · Page S4
45	Text S3. Analytical procedures · · · Page S5
46	
47	Figure S1. The UV-vis spectra of solution containing Fe(III) + GUA and solution
48	containing Fe(III)+ oxalate + GUA ····· Page S7
49	Figure S2. Mechanism for the dark reaction of GUA with Fe(III) ions Page S8
50	Figure S3. The Fe-catalyzed photooxidation kinetics of GUA in the presence of
51	oxalate and in the absence of oxalate ····· Page S9
52	Figure S4. The Fe-catalyzed photooxidation kinetics of NB in the presence of oxalate
53	and in the absence of oxalate·····Page S10
54	Figure S5. Effect of oxalate concentration on the Fe(III)-oxalate mediated
55	photooxidation kinetics of GUA ·····Page S11
56	Figure S6. Mole-fraction distribution of the Fe(III) species ····· Page S12
57	Figure S7. Effect of Fe(III) concentration on the Fe(III)-oxalate mediated
58	photooxidation kinetics of GUA ·····Page S13
59	Figure S8. Effect of solution pH on the Fe(III)-oxalate mediated photooxidation
60	kinetics of GUA ·····Page S14
61	Figure S9. Effect of the presence of oxygen on the formation of H ₂ O ₂ in irradiated
62	ferrioxalate system ·····Page S15
63	Figure S10. Van Krevelen diagram of the oxidative products of GUA ······Page S16
64	Figure S11. GC-MS spectra of methanol formed from the photooxidation of GUA
65	Page S17
66	
67	Table S1. The products formed through the aqueous-phase reactions of GUA with OH
68	Page S18
69	
70	References · · · · Page S23

Text S1. Materials and reagents

71

72

73

74

75

76

77

78

79

80

81 82

83 84

All chemicals were analytical grade and were used as received. The water employed was distilled and deionized by a Millipore purification system (Barnstead NANO Pure, USA). Chemical agents of iron (III) chloride anhydrous (FeCl₃), ethanedioic acid dehydrate (H₂C₂O₄·2H₂O), guaiacol (C₇H₈O₂), nitrobenzene (C₆H₅NO₂), hydrochloric acid (HCl), sodium hydroxide (NaOH) were purchased from Sinopharm Chemical Reagent Co. Ltd. (Shanghai, China). Sodium phosphate dibasic (Na₂HPO₄), sodium phosphate monobasic (NaH_2PO_4) , N,N-Diethyl-pphenylenediamine sulfate salt, peroxidase from horseradish were purchased from Sigma-Aldrich. Glassware and quartzware were cleaned with a 10% HCl solution, followed by rinsing with deionized water. All solutions were prepared using deionized water.

Text S2. Additional experimental details

Except where noted, the photochemical reactions were carried out under the following experimental conditions: initial [Fe(III)] = $20~\mu M$, initial [guaiacol] = $50~\mu M$ and initial oxalate concentration [H₂C₂O₄] = $250~\mu M$ at the solution pH 3.0 with 100 mL solution, all solutions were saturated with air. Moreover, the ionic strength of each experiment was 2.58×10^{-3} mol kg⁻¹ for NaCl. A tenfold (molar) excess of oxalate/Fe(III) was used for the experiment to ensure complete complexation of Fe(III) by oxalate [1]. These concentrations reflect the concentrations of these species found in real atmospheric liquid phases. The pH value of the solution was monitored by a pH meter during the whole experiment. The initial pH of solution was adjusted to the desired pH with either diluted HCl or NaOH solution prior to the photochemical reactions, when necessary, the pH was kept constant by addition of diluted HCl or NaOH solution. The pH variations during all experiments were < \pm 0.2 pH units. The dark control experiments were performed in a flask containing the necessary agents and the flask was covered with aluminum foil. Aliquots of the sample (1mL) were withdrawn at given time intervals and were analyzed by HPLC.

Text S3. Analytical Procedures

S3.1 HPLC analysis

The concentration of guaiacol was determined using a HPLC [Agilent (1260), Phenomenex Luna-18 C18 column (250 \times 4.60 mm, 5 μm), photodiode array detector (DAD)] with a flow rate of 1 ml/min and detection wavelength of 274 nm. The mobile phase consisted of 40/60 (v/v) acetonitrile/water acidified with trifluoroacetic acid (TFA, 0.05%). The injection volume was 20 μl and the retention time of guaiacol was 6.45 min. The concentration of nitrobenzene was determined using a HPLC [Agilent (1260), Phenomenex Luna-18 C18 column (250 \times 4.60 mm, 5 μm), photodiode array detector (DAD)] with a flow rate of 1 ml/min and detection wavelength of 267 nm. The mobile phase consisted of 60/40 (v/v) acetonitrile/water acidified with trifluoroacetic acid (TFA, 0.05%). The injection volume was 20 μl and the retention time of nitrobenzene was 7.22 min.

S3.2 HRMS coupled with HPLC analysis

The analysis of oxidation products was carried out using a Q Exactive mass spectrometer (Orbitrap, Thermo Fisher Scientific, mass resolution= 140000 FWHM) equipped with UltiMate 3000 UHPLC. The samples were separated on a Waters XBridge C₁₈ column (2.1 × 100 mm, 3.5 µm) equipped with a guard column (2.1× 5 mm) of same packing material. The mobile phase consisted of A: 0.1% acetic acid in H₂O and B: 0.1% acetic acid in CH₃CN, with a gradient elution of 5% B for 3min, followed by a linear increase to 100% B within 27 min, back to 5% B in 30 min. The flow rate was 0.3 ml/min and injection volume was 5 µl. The mass spectra (m/z 90-500) were obtained in negative ion mode with electrospray ionization technology (ESI). The major ion peaks were assigned as deprotonated formulas $C_cH_{h-1}O_0^-$ ($c \ge 4$, $h \ge 4$, $0 \le o \le 10$) using Thermo Xcalibur software (version 2.2). The mass accuracy limit was set as ± 5 ppm, and the double bond equivalent value (DBE) ought to be less than 9. The DBE is calculated as c+1-0.5h for an ion of $C_cH_{h-1}O_0^-$.

S3.3 UV-vis analysis and H₂O₂ analysis

A YOKE UV1901 diode array spectrophotometer utilizing both its tungsten lamp and deuterium lamp was used for UV-VIS absorption measurements. A 1 cm quartz cuvette was used for measuring absorbance and the deionized water was utilized as the spectroscopic blank. The detection range of the entire spectrum was between 190-1100 nm. The concentration of H₂O₂ formed during the course of irradiation was determined by a modified method based on the horseradish peroxidase (POD) catalyzed oxidation of N,N-diethyl-p-phenylenediamine sulfate salt (DPD) by H₂O₂ [2].

A series of standard solutions of H_2O_2 at concentrations of 0.1, 0.5, 1.0, 5.0, 10.0 μ M were freshly prepared by diluting a stock solution of H_2O_2 (9.79 M). 1 mL (2.46×10⁻² M Na₂HPO₄/0.263 M NaH₂PO₄) buffer solution was added to 4 mL of a standard solution or an irradiated solution followed by addition of 50 μ L 1% (w/w) DPD in 0.1 N H₂SO₄ and 50 μ L 100% (w/w) POD solution (specific activity of 100 units mg⁻¹) in rapid succession. The absorbance of the sample was measured at 552 nm at 40 \pm 5 s after the addition of the POD. The detection limit of H₂O₂ is 0.1 μ M.

S3.4 GC-MS analysis

For gas chromatography/mass spectrometry (GC-MS) analyses, the sample solution after reaction was directly injected into a Thermo FOCUS DSQ GC-MS, equipped with a HP-INNOWax fused-silica capillary column ($30 \text{ m} \times 0.25 \text{ mm ID}$, 0.25 µm). The conditions utilized for GC-MS analysis were: carrier gas flow 1 mL/min (He), injector temperature 250 °C, the column temperature was initially held at for 60 °C for 3min, then raised to 300 °C at a rate of 30 °C min⁻¹, with a final holding time of 2 min. The mass spectra were scanned from m/z 29-400 with electron impact ionization technology (EI). Data acquisition and analysis were carried out by using the Thermo Xcalibur software (version 2.2). Compounds were identified using the NIST Mass Spectral Library (National Institute of Standards and Technology, Washington DC, USA).

S3.5 pH measurement

pH value was measured by a SX-610 pH-meter (Shanghai San-Xin) equipped with a SX615 combination glass electrode with saturated KCl as inner reference solution, and calibrated with pH 4, 7, 10 standard buffers (Shanghai San-Xin).

S3.6 Irradiance measurements

Irradiance measurements at the surface of solutions was carried out by using a CEL-NP 2000 optical power meter (Beijing CEAULIGHT).

S3.7 Equilibrium calculation

All speciation calculations in this work were carried out with a chemical equilibrium calculation program-Visual MINTEQ at fixed Fe(III) concentration of 20 μ M at pH 3.0, 25 °C and the ionic strength was 2.58×10^{-3} mol kg⁻¹.

_, 0

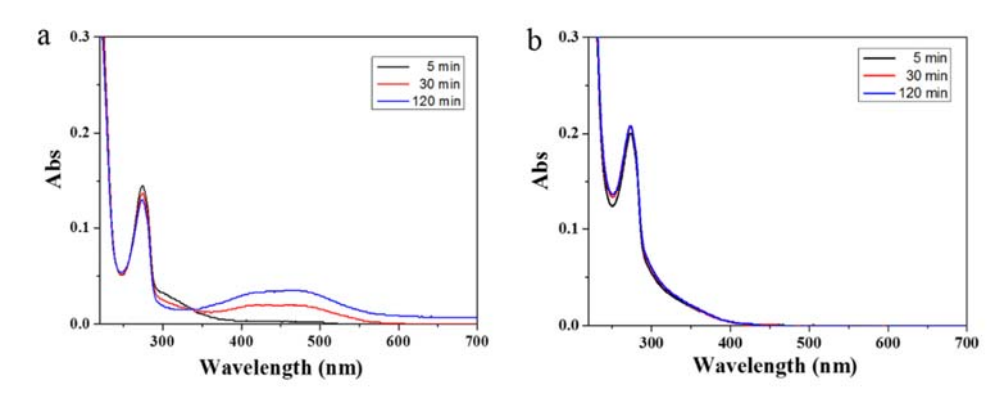


Figure S1. The UV-vis spectra of solution containing 20 μ M Fe(III) and 50 μ M GUA (a) and solution containing 20 μ M Fe(III), 250 μ M oxalate and 50 μ M GUA (b) as a function of time at pH = 3 \pm 0.1.

Fe(III) +
$$H_3CO$$

Fe(III) + H^+ + H_3CO

radical coupling

$$H_3CO$$
 H_3CO
 H_3CO
 OH
 OH

Figure S2. Proposed mechanism for the dark reaction of GUA with Fe(III) and the formation of oligomers through the radical recombination reactions in aqueous phase. Adopted from ref [3].

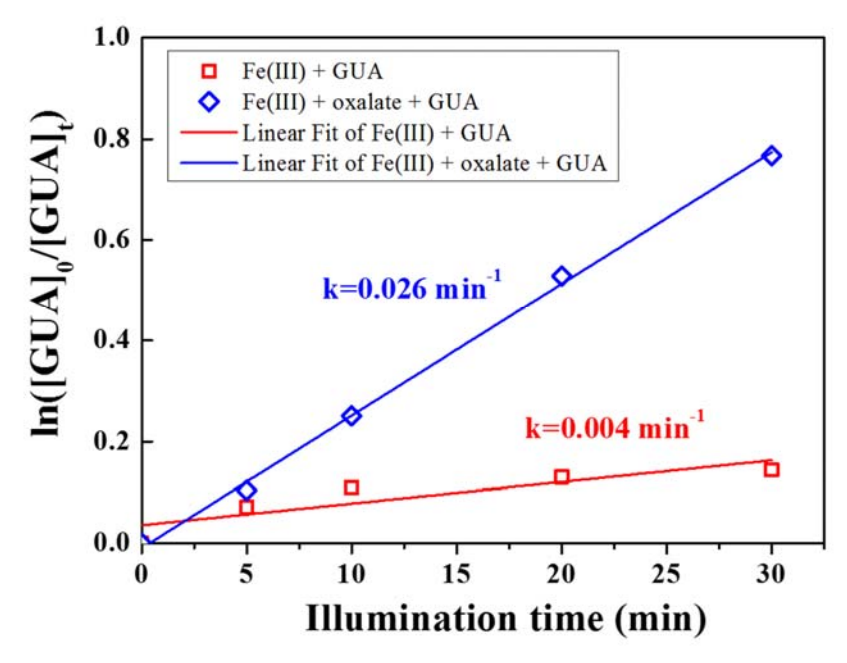


Figure S3. The Fe-catalyzed photooxidation kinetics of GUA in the presence of oxalate (red line) and in the absence of oxalate (black line). Fe(III)] $_0 = 20 \mu M$, [GUA] $_0 = 50 \mu M$, [Oxalate] $_0 = 250 \mu M$, pH = 3.0 ± 0.1 , air saturated solution.

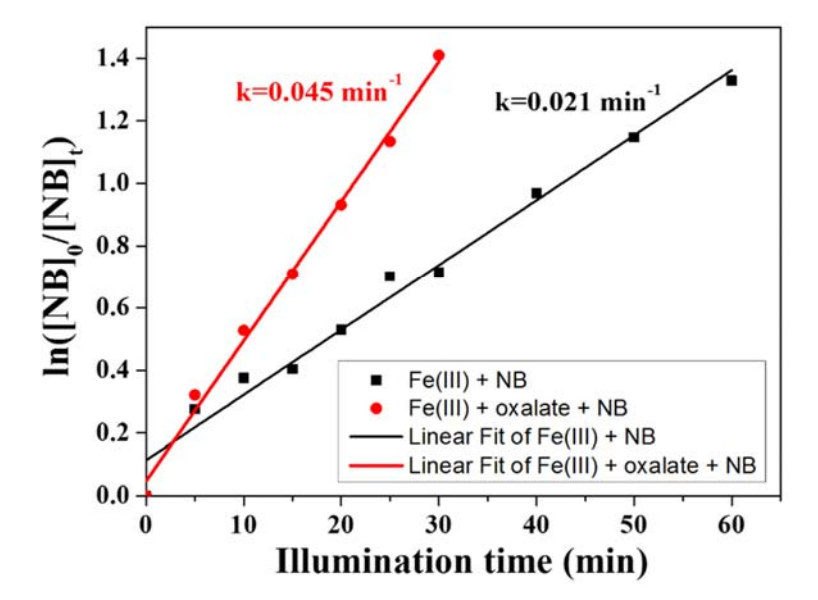


Figure S4. The Fe-catalyzed photooxidation kinetics of NB in the presence of oxalate (red line) and in the absence of oxalate (black line). Fe(III)] $_0 = 20 \mu M$, [NB] $_0 = 50 \mu M$, [Oxalate] $_0 = 250 \mu M$, pH = 3.0 ± 0.1 , air saturated solution.

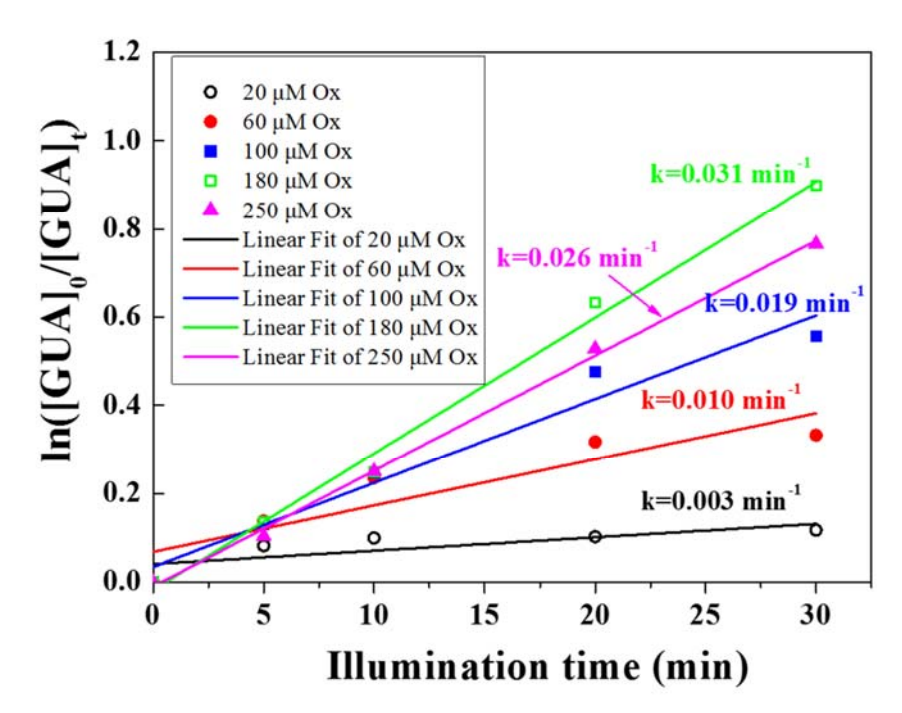


Figure S5. Effect of oxalate concentration on the photooxidation kinetics of GUA in the presence of Fe(III)-oxalate complexes. Fe(III)] $_0$ = 20 μ M, [GUA] $_0$ = 50 μ M, pH = 3.0 ± 0.1, air saturated solution. Ox represents oxalate.

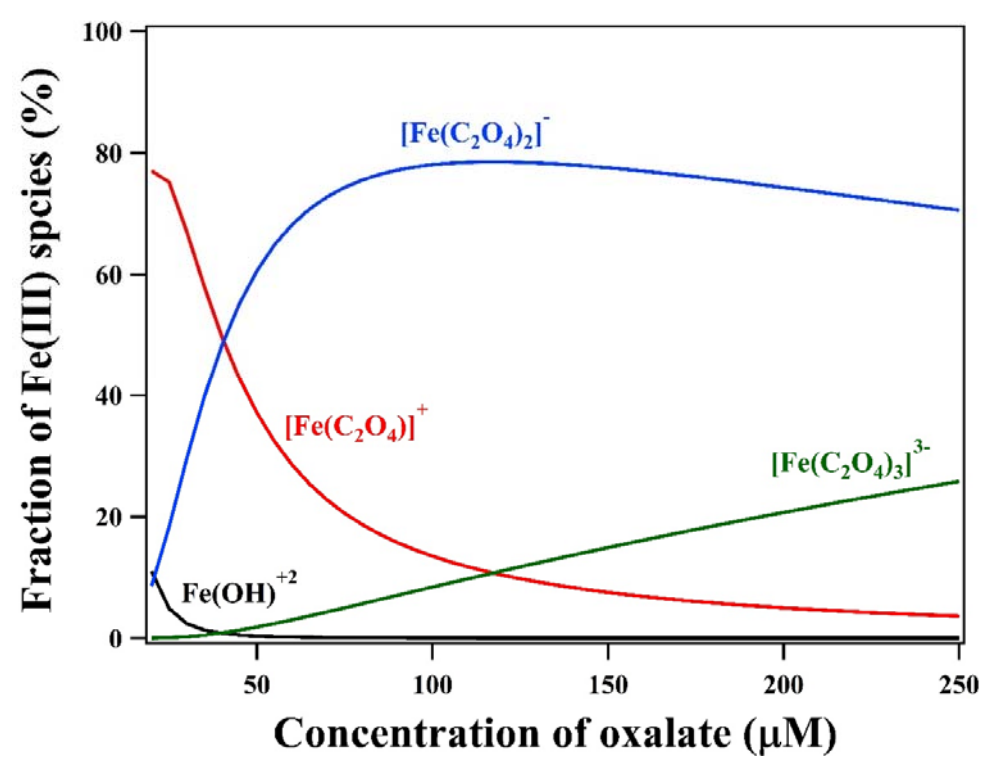


Figure S6. Mole-fraction distribution of the Fe(III) species (25 °C, pH 3.0, [Fe(III)] = $20 \mu M$, the ionic strength of was 2.58×10^{-3} mol kg⁻¹).

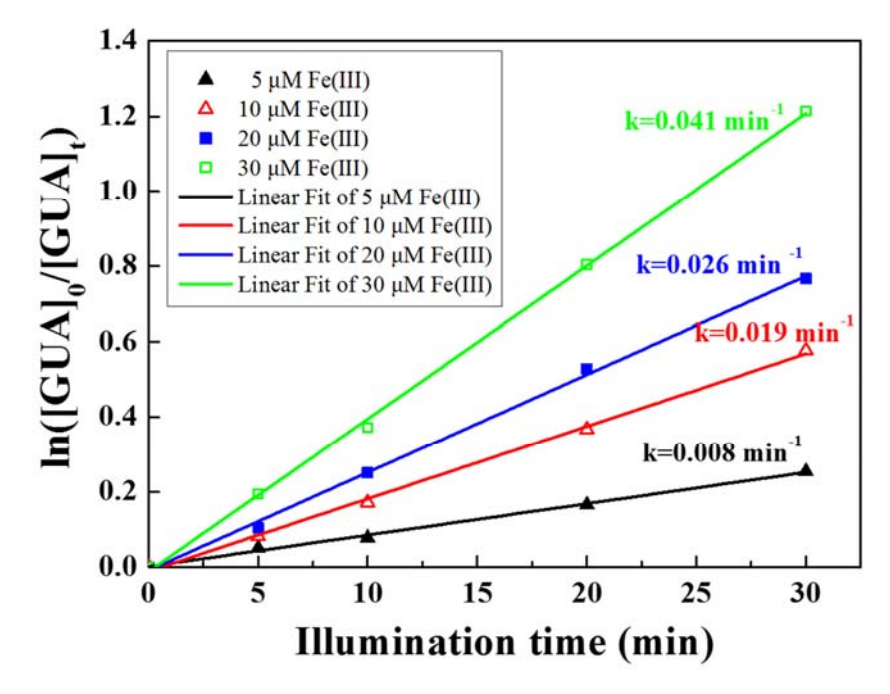


Figure S7. Effect of Fe(III) concentration on the photooxidation kinetics of GUA in the presence of Fe(III)-oxalate complexes. [Oxalate] $_0$ = 250 μ M, [GUA] $_0$ = 50 μ M, pH = 3.0 ± 0.1, air saturated solution.

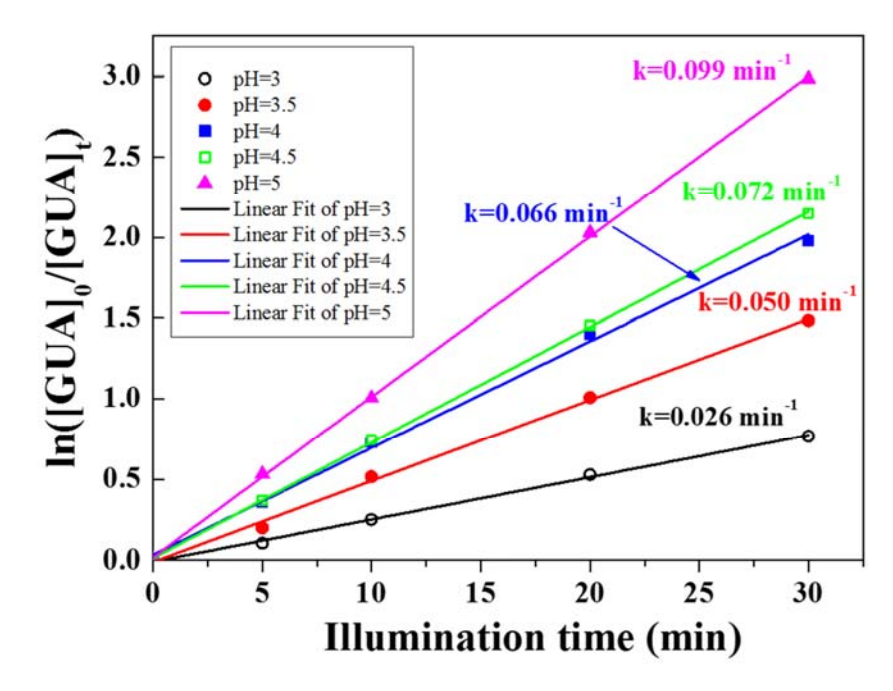


Figure S8. Effect of solution pH on the photooxidation kinetics of GUA in the presence of Fe(III)-oxalate complexes. Fe(III)] $_0 = 20 \, \mu M$, [Oxalate] $_0 = 250 \, \mu M$, [GUA] $_0 = 50 \, \mu M$, air saturated solution.

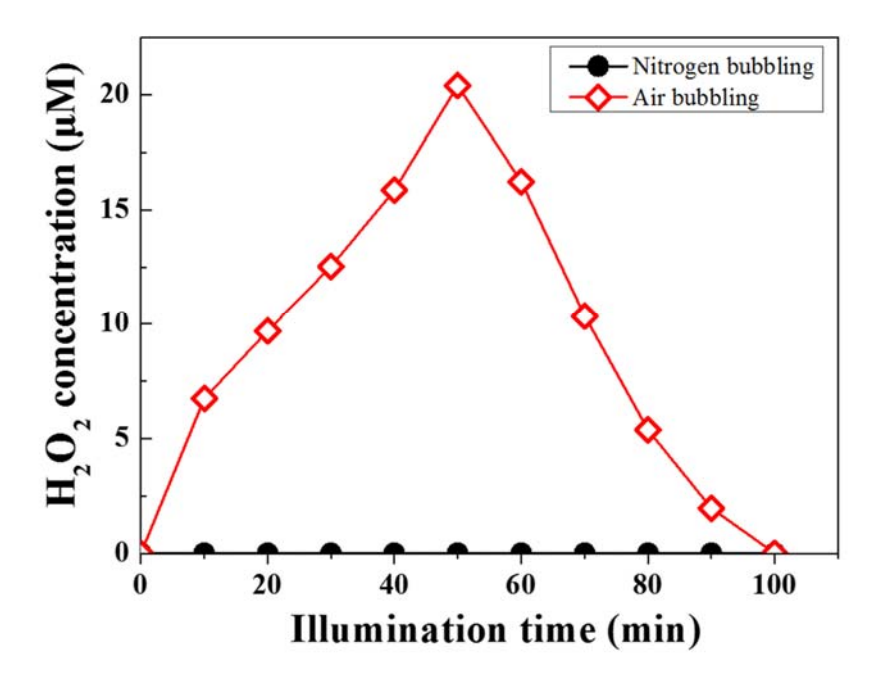


Figure S9. Effect of the presence of oxygen on the formation of H_2O_2 in irradiated ferrioxalate system. $[Fe(III)]_0 = 20 \mu M$, $[Oxalate]_0 = 250 \mu M$, $[GUA]_0 = 50 \mu M$, $pH = 3.0 \pm 0.1$, air bubbling (red line), nitrogen bubbling (blue line).

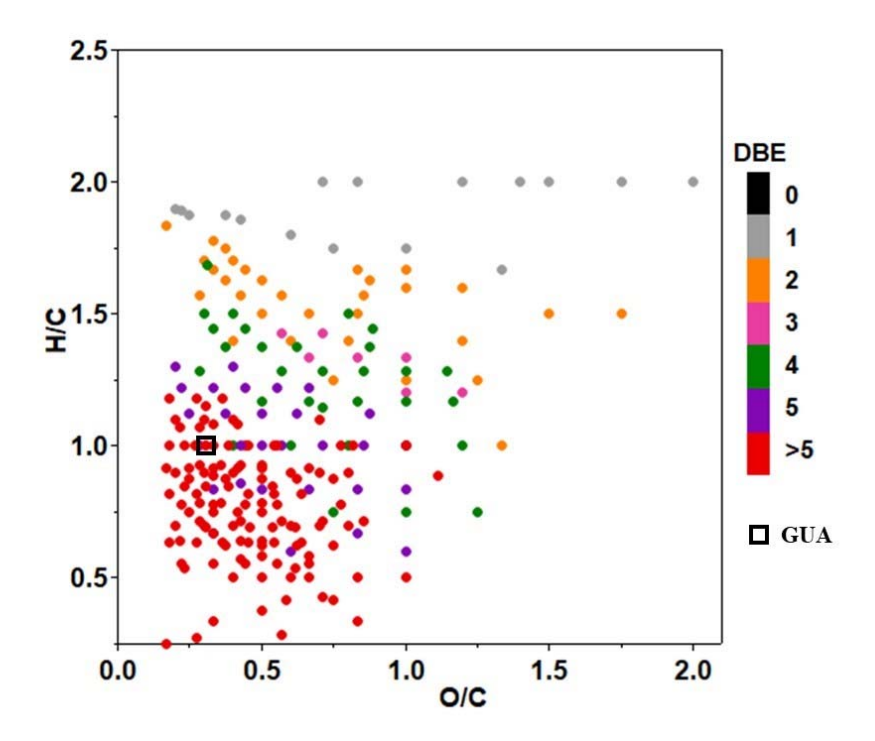


Figure S10. Van Krevelen diagram of the oxidative products of GUA from the photo/ferrioxalate system: [Fe(III)] $_0$ = 20 μ M, [Oxalate] $_0$ = 250 μ M, [GUA] $_0$ = 50 μ M, pH = 3.0 ± 0.1, air bubbling

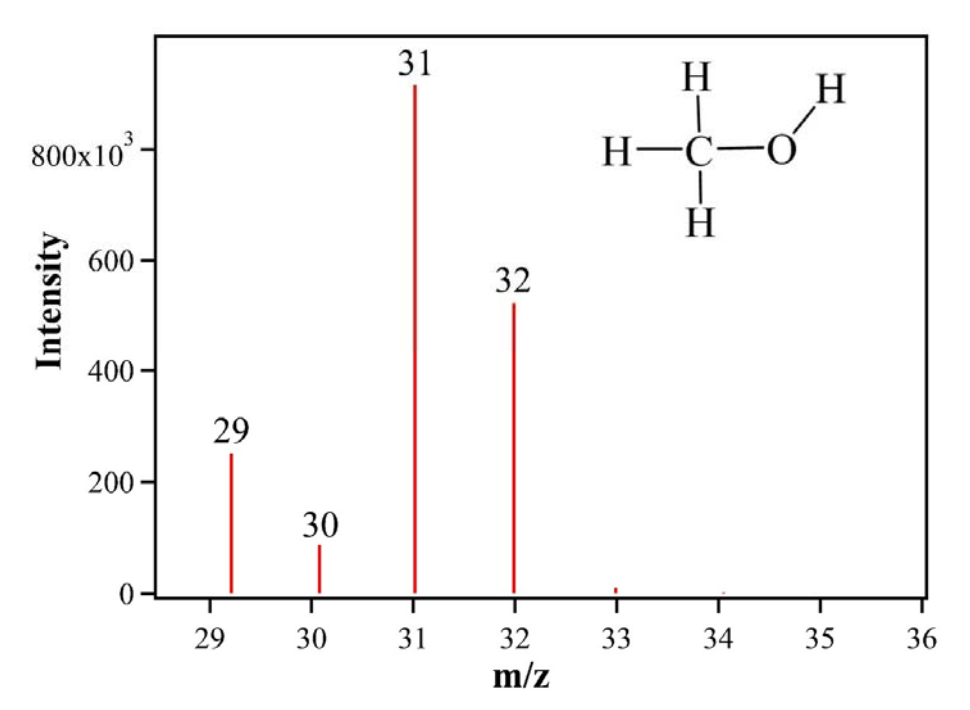


Figure S11. GC-MS spectra of methanol formed from the photooxidation of GUA in the presence of Fe(III)-oxalate system. [Fe(III)] $_0 = 20 \mu M$, [Oxalate] $_0 = 250 \mu M$, [GUA] $_0 = 50 \mu M$, pH = 3.0 ± 0.1 , air bubbling.

Table S1. The products formed through the aqueous-phase reactions of GUA with OH generated by photolysis of Fe(III)-oxalate system identified with (–) Orbitrap MS. The rank is based on the peak abundance of the ions.

No.	Ion	Molecular	Proposed	The	No.	Ion	Molecular	Proposed	The
	composition	Formula	Structure	compound'		composition	formula	structure	compound'
	(m/z)			s code in		(m/z)			s code in
				the Fig. 5 or					the Fig. 5 or
				6)					6)
	$C_6H_5O_2^-$	$C_6H_6O_2$	ÓН	Fig. 5, A ₁₅		$C_4H_3O_4^-$	C ₄ H ₄ O ₄	O	
1	(109.02924)		ОН		2	(115.00338)		н-С Он	
								Н С=С	
	C14H13O4	C14H14O4	OH H ₃ CO	Fig. 5, A ₁₈	_	C ₁₄ H ₁₃ O ₄ -	C14H14O4	H ₃ CO OH	Fig. 5, A ₁₆
3	(245.08215)				4	(245.08215)			
								O OCH ₃	
			OCH₃						
	C ₁₂ H ₁₁ O ₆ -	C12H12O6	O H O			C ₈ H ₅ O ₄ -	C ₈ H ₆ O ₄	O	
5	(251.05622)		HO-C-C-C-C-C		6	(165.01893)		С-н	
			ОН						
			OCH ₃					О-С-Н	

7	C7H5O3 ⁻ (137.02408)	C7H6O3	О О—С—Н ОН		8	C7H5O3 ⁻ (137.02408)	C7H6O3	OCH ₃	Fig. 5, A9
9	C ₅ H ₅ O ₄ ⁻ (129.01919)	C5H6O4	$\begin{array}{c} O \\ H-C \\ C = C \\ O \\ O \end{array}$	Fig. 6, B ₁₀	10	C ₅ H ₅ O ₄ ⁻ (129.01919)	C5H6O4	O O H H ₃ CO-C C C C	Fig. 6, B ₁₄
11	C ₁₂ H ₉ O ₆ ⁻ (249.04060)	C ₁₂ H ₁₀ O ₆	но он но он		12	C ₇ H ₇ O ₅ ⁻ (171.02946)	C7H8O5	OCH ₃ OH OH	
13	C ₇ H ₇ O ₅ - (171.02946)	C7H8O5	O H-C H C—C—C—H OCH ₃ OH	Fig. 6, B ₅	14	C ₉ H ₇ O ₅ ⁻ (195.02994)	C9H8O5	ОСН ₃ О—С—С—ОН О О	Fig. 5, A ₁
15	C ₆ H ₃ O ₃ - (123.00863)	C6H4O3	ООН	Fig. 5, A ₁₄	16	C ₉ H ₅ O ₆ ⁻ (209.00876)	C9H6O6	О О-С-Н О-С-С-ОН О О	

17	C ₁₀ H ₅ O ₆ ⁻ (221.00934)	C ₁₀ H ₆ O ₆	O O O O O O O O O O O O O O O O O O O		18	C ₇ H ₇ O ₆ ⁻ (187.02462)	C7H8O6	HO OH OH	
19	C ₇ H ₇ O ₆ ⁻ (187.02462)	C7H8O6	OCH ₃ OH OH		20	C ₆ H ₅ O ₅ ⁻ (157.01368)	C ₆ H ₆ O ₅	ОН	
21	C ₆ H ₅ O ₃ - (125.02417)	C6H6O3	ОН		22	C ₇ H ₉ O ₆ ⁻ (189.04041)	C7H10O6	OCH ₃ OH OH	
23	C ₉ H ₇ O ₄ ⁻ (179.03482)	C9H8O4	OCH ₃ O O O U U U U U U U U U U U U U U U U		24	C ₆ H ₅ O ₆ ⁻ (173.00883)	C ₆ H ₆ O ₆	ОН ОН ОН	
25	C ₇ H ₇ O ₃ ⁻ (139.03976)	C7H8O3	OCH ₃ OH OH	Fig. 5, A ₈	26	C ₇ H ₇ O ₃ ⁻ (139.03976)	C7H8O3	OCH ₃ OH	Fig. 5, A7

27	C ₁₀ H ₉ O ₈ ⁻ (257.03048)	C10H10O8	O O HO-C H H C-OH C=C C=C H ₃ CO C-C OCH ₃		28	C ₆ H ₅ O ₄ ⁻ (141.01885)	C6H6O4	ОН	
29	C ₇ H ₉ O ₅ ⁻ (173.04529)	C ₇ H ₁₀ O ₅	OCH ₃ OH OH	Fig. 5, A4	30	C ₇ H ₉ O ₅ ⁻ (173.04529)	C7H10O5	H ₃ CO OH OH	
31	C ₇ H ₉ O ₈ ⁻ (221.03025)	C7H10O8	HOO OCH ₃ OH OH		32	C ₁₂ H ₉ O ₄ ⁻ (217.05085)	C12H10O4	но он	
33	C ₄ H ₃ O ₅ ⁻ (130.99834)	C ₄ H ₄ O ₅	О Н-С С=С НО С-ОН		34	C7H9O4 ⁻ (157.05014)	C7H10O4	OCH ₃ OH OH	
35	C ₇ H ₉ O ₇ ⁻ (205.03497)	C7H10O7	OCH ₃ OH OH	Fig. 5, A ₆	36	C ₇ H ₉ O ₇ ⁻ (205.03497)	C7H10O7	HO OCH ₃ OH OH	

37	C ₉ H ₅ O ₅ ⁻ (193.01420)	C9H6O5	O O O O O O O O O O O O O O O O O O O		38	C ₁₂ H ₉ O ₅ ⁻ (233.04566)	C12H10O5	но он	
39	C ₁₄ H ₁₁ O ₄ ⁻ (243.06636)	C14H12O4	O OCH ₃	Fig. 5, A ₁₇	40	C ₁₄ H ₁₃ O ₅ ⁻ (261.07693)	C14H14O5	HO OH H ₃ CO—OCH ₃ OH	

References:

- [1] Weller C, Horn S, Herrmann H. Effects of Fe (III)-concentration, speciation, excitation-wavelength and light intensity on the quantum yield of iron (III)-oxalato complex photolysis. Journal of Photochemistry and Photobiology A: Chemistry. 2013;255:41-9.
- [2] Bader H, Sturzenegger V, Hoigne J. Photometric method for the determination of low concentrations of hydrogen peroxide by the peroxidase catalyzed oxidation of N, N-diethyl-p-phenylenediamine (DPD). Water Research. 1988;22(9):1109-15.
- [3] Lavi A, Lin P, Bhaduri B, Carmieli R, Laskin A, Rudich Y. Characterization of Light-Absorbing Oligomers from Reactions of Phenolic Compounds and Fe (III). ACS Earth and Space Chemistry. 2017;1(10):637-46.